NASA Contractor Report 3142

The Use of Coherence Functions To Determine Dynamic Excitation Sources on Launch Vehicle Payloads

Stanley Barrett and Robert M. Halvorson

CONTRACT NAS1-14370
JUNE 1979

NASA

NASA Contractor Report 3142

The Use of Coherence Functions To Determine Dynamic Excitation Sources on Launch Vehicle Payloads

Stanley Barrett and Robert M. Halvorson
Martin Marietta Corporation
Denver, Colorado

Prepared for
Langley Research Center
under Contract NAS1-14370

National Aeronautics
and Space Administration

**Scientific and Technical
Information Branch**

1979

CONTENTS

	Page
Summary	1
Introduction	2
Symbols and Abbreviations	3
Discussion of Coherence Functions	5
Analysis of Three Input/Single Output System	15
Experimental Program	18
Discussion of Results	23
Phase I: Stationary Inputs	23
Phase II: Nonstationary Inputs	63
Conclusions	71
References	74

SUMMARY

The objective of the study described in this report was to evaluate the use of coherence functions for identifying the relative contributions of multiple dynamic inputs to the measured vibration response of spacecraft components under realistic conditions. Data for the study were generated by applying simultaneous vibratory and acoustic excitation of similar spectral content to a test model, which was a modified instrumentation truss from a Titan launch vehicle with a flat, lightly-loaded panel added to one bay to provide response data. Up to three inputs were used in tests conducted in an acoustically "live" room. Both independent and mutually coherent inputs were studied and stationary and nonstationary environments were simulated.

A digital computer program was written to analyze the test data. The mathematical approach was based on iterative computational algorithms developed recently by Bendat. This approach is simpler than earlier matrix methods and is thought to be more economical in terms of computer time.

It was demonstrated that the coherence function technique was effective in identifying and evaluating sources of excitation, for both correlated and noncorrelated cases, but only when the sources were stationary and only in the vicinity of strong structural responses. The investigation of nonstationary sources showed that the application of analytical techniques based on the assumption of stationarity did not give acceptable results, even for relatively slowly varying inputs.

To calculate coherence functions with high accuracy, it is necessary to use smoothed estimates of the associated auto and crosspectra. The effect of varying the number of data samples used in the smoothing or averaging process was briefly investigated.

INTRODUCTION

The situation frequently arises in the field of environmental dynamics in which it is desirable to identify and rank the dynamic sources contributing to the measured output of a system. A familiar case is the estimation of the relative severity of various noise sources making up the acoustic environment in a factory before applying noise reduction methods. A less familiar and more complex example is the problem of protecting a sensitive electronic assembly on a launch vehicle payload, which is being excited by simultaneous acoustic and vibration inputs; this can be solved more easily if the dynamicist knows how the various inputs contribute to the overall response. In this case, the payload itself may interact with the inputs because of its own dynamic characteristics.

A number of techniques are available for performing this source identification. If the sources are concentrated in narrow, independent frequency bands, frequency spectrum analysis is satisfactory and is frequently used. However, when the bandwidths of the various inputs overlap, as is often the case in launch vehicles, the resulting spectra can be ambiguous. In this situation, a time-domain approach can be applied, using auto- and cross-correlation functions. Unfortunately, there are some serious practical limitations inherent in correlation techniques, as discussed by Broch (Ref. 1); consequently, attention has been directed recently to using various forms of the coherence function to solve the problem. The coherence function is a frequency-domain function which provides the same basic information as the correlation function, but presents it in a more usable form and usually with improved resolution.

It may also be used to evaluate the fidelity of measured transfer functions - but this report concentrates on the application to solving the source identification problem.

The purpose of the investigation described here was to develop a practical technique for calculating the coherence functions associated with a structural assembly which is being excited by several inputs, so that the relative contributions of the inputs to the measured vibration response could be estimated. Similar work in this area was reported recently (Ref. 2) in which several sources of vibration that were causing an airborne antenna to malfunction were investigated using coherence functions, based on a matrix treatment. The current study is more general and used a nonmatrix computational technique developed recently by Bendat (Ref. 3) which should be more economical than the matrix approach. Testing was performed on a typical structural assembly, using several input/output conditions, to obtain data with which to develop the technique.

SYMBOLS AND ABBREVIATIONS

accel	accelerometer
E { }	expectation operator
dB	decibel
f	frequency parameter
g	acceleration unit
$G_{ii}(f)$	auto-spectrum of $x_i(t)$
$G_{yy}(f)$	auto-spectrum of y(t)
$G_{nn}(f)$	auto-spectrum of n(t)
$G_{ij}(f)$	cross-spectrum of $x_i(t)$ with $x_j(t)$
$G_{iy}(f)$	cross-spectrum of $x_i(t)$ with y(t)
G*(f)	complex conjugate of G(f)
h(t)	impulse response
H(f)	Fourier transform of h(t)
Hz	Hertz (cycles per second)
i	index, i = i,2,3,...r,...p
j	index, j = 1,2,3,...r,...p
L(f)	frequency response function
MCF	multiple coherence function
n(t)	noise input
N(f)	Fourier transform of n(t)
opt	optimum
OASPL	overall sound pressure level
OCF	ordinary coherence function
p	maximum value of i or j
PCF	partial coherence function
Ref.	reference
RMS	root mean square
sec	seconds
t	time
$x_i(t)$	ith input
$X_i(f)$	Fourier transform of $x_i(t)$

$y(t)$	output
$Y(f)$	Fourier transform of $y(t)$
γ^2_{ij}	OCF between $x_i(t)$ and $x_j(t)$
γ^2_{iy}	OCF between $x_i(t)$ and $y(t)$
$\gamma^2_{y:x}$	MCF between set of inputs $x(t)$ and output $y(t)$
$\gamma^2_{iy.(i+1)(i+2)...}$	PCF between input $x_i(t)$ and output $y(t)$ after removing the effects of correlated inputs $x_{i+1}(t)$ $x_{i+2}(t)...$
ε	RMS error

DISCUSSION OF COHERENCE FUNCTIONS

Three forms of the coherence function are used in this report; these are the Ordinary Coherence Function (OCF), the Multiple Coherence function (MCF) and the Partial Coherence Function (PCF). The PCF is sometimes referred to as the Conditional Coherence Function in the literature. Other kinds of coherence functions have been defined (see Ref. 4) but will not be discussed here. The OCF, MCF, and PCF are all measures of the linear dependance between spectral components of random processes, and are real valued functions of frequency varying in magnitude between zero and one.

Consider a set of stationary random inputs $x_i(t)$ $(i = 1,2,3,\ldots p)$ and one output $y(t)$, acting on the constant parameter linear system shown below:

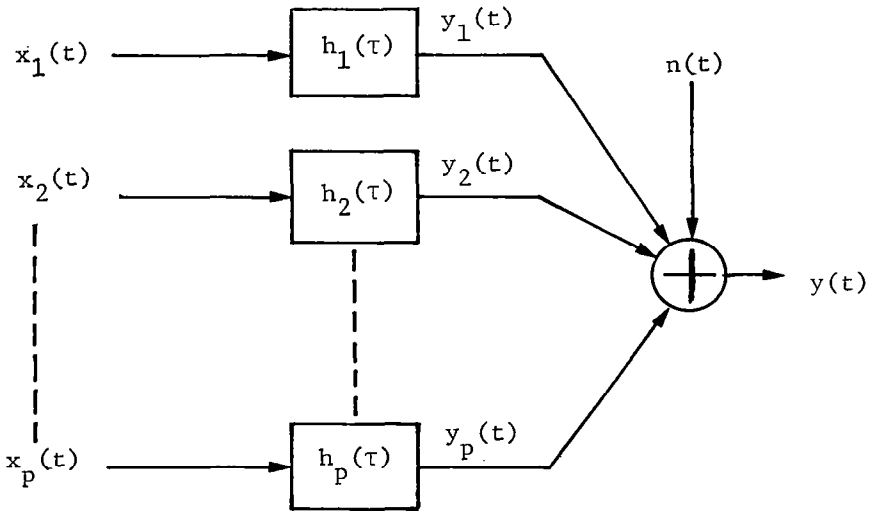

Figure 1. - Multiple input/single output system.

The local outputs $y_i(t)$ are responses to $x_i(t)$ and are defined by the impulse response or weighting functions $h_i(\tau)$:

$$Y_i(t) = \int_0^\infty h_i(\tau)\, x_i(t-\tau)\, d\tau \qquad (1)$$

The "noise" term [n(t)] shown in Figure 1 is intended to account for any deviations from the ideal model; it would include measurement noise at the output, time delays in the measured data, nonlinear effects, statistical errors, etc. We assume n(t) to be statistically independent of the total measured output y(t).

Thus, we have

$$y(t) = y_1(t) + y_2(t) + \ldots\ldots + y_p(t) + n(t) \qquad (2)$$

Conversion of equations (1) and (2) from the time domain to the frequency domain by Fourier transforms results in

$$Y_i(f) = H_i(f)\, X_i(f) \qquad (3)$$

$$\begin{aligned} Y(f) &= Y_1(f) + Y_2(f) + \ldots\ldots + Y_p(f) + N(f) \qquad (4) \\ &= H_1(f)\, X_1(f) + \ldots\ldots + H_p(f)\, X_p(f) + N_{(f)} \end{aligned}$$

The spectral density functions associated with the time functions used are

$G_{ii}(f)$ = auto-spectrum of $x_i(t)$

$G_{yy}(f)$ = auto-spectrum of $y(t)$

$G_{nn}(f)$ = auto-spectrum of $n(t)$

$G_{ij}(f)$ = cross-spectrum of $x_i(t)$ with $x_j(t)$

$G_{iy}(f)$ = cross-spectrum of $x_i(t)$ with $Y(t)$

The cross-spectrum of n(t) with y(t), $G_{ny}(f)$, could also be defined, but would vanish since n(t) and y(t) were assumed to be statistically independent. Note that we are using one-sided spectra, involving only positive frequencies. Theoretical studies often work with two-sided spectra, but since the correction is a factor of two that would always cancel out in the equations because of the way the spectra are used, we can safely use the more physically meaningful one-sided spectra immediately.

In what follows, most quantities used will be functions of frequency, but we shall generally omit the (f) dependency for brevity in notation.

The auto-spectrum of the total output is

$$G_{yy} = |H_1|^2 G_{11} + |H_2|^2 G_{22} + \cdots + |H_p|^2 G_{pp} + G_{nn} \quad (5)$$

But $|H_i|^2 G_{ii} = H_i H_i^* G_{ii}$

and $H_i G_{ii} = G_{iy}$

$\therefore H_i^* G_{ii} = G_{iy}^* = G_{yi}$

$\therefore |H_i|^2 G_{ii} = H_i G_{yi}$

so that equation (5) may be written

$$G_{yy} = \sum_{i=1}^{p} H_i G_{yi} + G_{nn} \quad (6)$$

The ordinary coherence function between any two inputs $x_i(t)$ and $x_j(t)$ is given by

$$\gamma_{ij}^2 = \frac{|G_{ij}|^2}{G_{ii} G_{jj}} \quad (7)$$

If the inputs are completely independent, the OCF will vanish for all combinations of i and j, since G_{ij} will be zero. Thus, any variation from zero indicates mutual coherence between the inputs. Note that $\gamma_{ij}^2 = 1$ would mean that x_i and x_j contain redundant information and one of the inputs should be eliminated from the model.

The OCF between any input $x_i(t)$ and the total output y(t) is

$$\gamma_{iy}^2 = \frac{|G_{iy}|^2}{G_{ii} G_{yy}} \quad (8)$$

In this case, $\gamma_{iy}^2 = 1$ implies that the other inputs are not contributing to the output and the model should be viewed as a single input/single output system.

If the inputs are completely independent the sum of the input-output OCFs should be unity for all frequencies. When this result is not obtained, it means that noise is present in the input or output data, or other inputs exist which have not been included, or the system is nonlinear. The OCF γ_{iy}^2 shows the proportion of the total output resulting from $x_i(t)$; the actual output power contributed by $x_i(t)$ is given directly by $\gamma_{iy}^2 G_{ii}$.

The multiple coherence function shows the CF relationship between the complete set of inputs $x_1(t)$, $x_2(t)$,... $x_p(t)$ and the total output $y(t)$. It can be used as a diagnostic tool, to examine how closely an assumed model matches the actual system. A physical interpretation of the MCF concept may be obtained as follows:

Let $\hat{y}(t)$ = predicted output from an ideal model

$y(t)$ = actual measured output

$n(t)$ = effects causing deviations = $y(t)-\hat{y}(t)$

$G_{\hat{y}\hat{y}}$, G_{yy} and G_{nn} = corresponding auto-spectra, so that

$$G_{yy} = G_{\hat{y}\hat{y}} + G_{nn} \tag{9}$$

The MCF is defined as

$$\gamma^2_{x:y} = \frac{G_{\hat{y}\hat{y}}}{G_{yy}} = \frac{G_{yy}-G_{nn}}{G_{yy}} \tag{10}$$

Since both $G_{\hat{y}\hat{y}}$ and G_{nn} are real and positive-valued, G_{yy} can never be less than $G_{\hat{y}\hat{y}}$ so that the inequality $0 \leq \gamma^2_{y:x} \leq 1$ is always satisfied. Under ideal conditions, the MCF will be identically equal to unity for all frequencies.

If all the inputs are independent, the MCF will equal the sum of the individual input-output OCFs:

$$\gamma^2_{x:y} = \gamma^2_{1y} + \gamma^2_{2y} + \ldots + \gamma^2_{py} \tag{11}$$

This equation does not apply if the inputs have some degree of mutual coherence; however, a similar relationship can be developed between the MCF and various partial coherence functions. Before the PCFs can be calculated the inputs must be modified or "conditioned" to remove the coupling effects caused by the lack of independence between the inputs. Each PCF will then show the proportion of the output caused by a specific input, with the effects of all other inputs eliminated.

Special notation is used to show that the data records have been conditioned. Thus, for example, $x_{3.12}(t)$ indicates that input $x_3(t)$ has been conditioned on $x_1(t)$ and $x_2(t)$ to eliminate their effects. The corresponding auto-spectrum would be $G_{33.12}$. The auto-spectrum of the output after conditioning on $x_1(t)$ and $x_2(t)$ would be $G_{yy\cdot 12}$. The PCF between $x_3(t)$ and $y(t)$, conditioned on $x_1(t)$ and $x_2(t)$, is given by

$$\gamma^2_{3y.12} = \frac{|G_{3y.12}|^2}{G_{33.12}\, G_{yy.12}}$$

Thus, the PCF between the preconditioned quantities is equivalent to the OCF between the postconditioned quantities.

The numerical conditioning process is quite complicated for a multiple input system. Matrix methods have been developed (Refs. 4, 5, 6) and an application is described in reference 2. These methods are effective in keeping the computational process organized, but can be expensive in computer time, involving a considerable number of complex matrix inversions. An alternative method was developed recently by Bendat (Refs. 3, 7), in which iterative computational algorithms are used to calculate conditioned spectral density functions and partial coherence functions. The technique uses Fourier transforms of data records and performs the conditioning by removing an optimum least squares prediction of the "contaminating" inputs from each input in turn. A unique feature of Bendat's method is the use of "ordered" inputs. In this process, the original set of inputs records are rearranged in a particular order and then each record is conditioned on the preceding records. Thus, $x_1(t)$ is unchanged, $x_2(t)$ is conditioned on $x_1(t)$ to become $x_{2.1}(t)$, $x_3(t)$ is conditioned on $x_1(t)$ and $x_2(t)$ to become $x_{3.12}(t)$, and so on. The noise term n(t) is now equivalent to the output conditioned on all of the inputs. The output term y(t) remains in the model in its original nonconditioned form, however.

A revised model involving ordered, conditioned, frequency-domain inputs is shown in Figure 2.

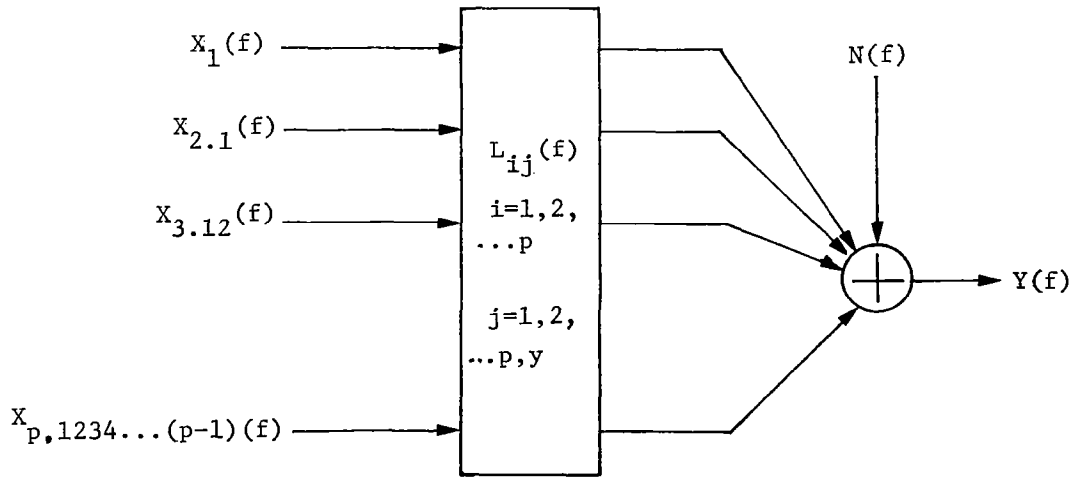

Figure 2. - Multiple input/single output system with ordered conditioned inputs.

The following procedure is used to establish the new order for the inputs:

(1) Calculate the OCF between each input $x_1(t)$ and the output $y(t)$.

(2) For the frequency range of primary interest, arrange the calculated OCFs in order of magnitude.

(3) The new $x_1(t)$ is the input which gives the highest OCF, $x_2(t)$ is the input giving the next highest OCF, and so on for the remaining inputs.

This gives a set of ordered inputs which now have to be conditioned by the process developed in reference 3 and summarized here.

The block labeled $L_{ij}(f)$ in the model represents frequency response functions connecting the conditioned inputs $x_{i.123\ldots(i-1)}(f)$ with each other and with the output $Y(f)$. The L_{ij} are used to estimate the effects of the preceding (i-1) inputs which are to be eliminated from the ith input in the interactive conditioning process. The L_{ij} must be optimized on the basis of minimizing the error in these estimates.

From the model, we can write

$$Y = \sum_{i=1}^{p} L_{iy} X_{i.123\ldots(i-1)} + N \tag{12}$$

$$\text{Let } N_{iy} = Y - L_{iy} X_{i.123\ldots(i-1)} \tag{13}$$

which is the difference between the total output y and the output due to the ith conditioned input passing through L_{iy}.

$$\begin{aligned}\text{Then } \left|N_{iy}\right|^2 &= \left|Y - L_{iy} X_{i.123\ldots(i-1)}\right|^2 \\ &= \left|Y\right|^2 - L_{iy}^{*} \left[X^{*}_{i.123\ldots(i-1)} Y\right] \\ &\quad - L_{iy} \left[Y^{*} X_{i.123\ldots(i-1)}\right] + L_{iy}^{*} L_{iy} \left|X_{i.123\ldots(i-1)}\right|^2 \end{aligned} \tag{14}$$

- where the asterisks indicate complex conjugates.
Taking expected values of both sides gives an expression for the mean square system error for any L_{iy}, in terms of auto-and cross-spectra of the conditioned input and the output:

$$E\{|N_{iy}|^2\} = \varepsilon^2$$
$$= G_{yy} - L_{iy}^{*} G_{iy.123\ldots(i-1)}$$
$$- L_{iy} G^{*}_{iy.123\ldots(i-1)} + L_{iy} L_{iy}^{*} G_{ii.123\ldots(i-1)} \qquad (15)$$

To minimize ε^2, differentiate equation (15) partially with respect to L_{iy} and equate to zero:

$$\frac{\partial(\varepsilon^2)}{\partial L_{iy}} = -G^{*}_{iy.123\ldots(i-1)} + L_{iy}^{*} G_{ii.123\ldots(i-1)} = 0$$

Taking complex conjugates and solving for the optimum L_{iy} gives

$$L_{iy}\ (\text{opt}) = \frac{G_{iy.123\ldots(i-1)}}{G_{ii\cdot 123\ldots(i-1)}} \qquad (16)$$

The optimum input/output frequency response functions for the model will thus be

$$L_{1y} = \frac{G_{1y}}{G_{11}}$$

$$L_{2y} = \frac{G_{2y\cdot 1}}{G_{22.1}}$$

$$L_{3y} = \frac{G_{3y\cdot 12}}{G_{33.12}}$$

.....etc.

In a similar manner, we can find the optimum frequency response functions connecting the coherent inputs, by setting y=j:

$$L_{ij}\ (\text{opt}) = \frac{G_{ij.123\ldots(i-1)}}{G_{ii.123\ldots(i-1)}} \qquad \begin{matrix} i = 1,2,\ldots.p \\ j > i \end{matrix} \qquad (17)$$

$$L_{12} = \frac{G_{12}}{G_{11}} \qquad L_{13} = \frac{G_{13}}{G_{11}} \ \ldots\ldots$$

$$L_{23} = \frac{G_{23.1}}{G_{22.1}} \qquad L_{24} = \frac{G_{24.1}}{G_{22.1}} \ \ldots\ldots$$

. . . . . .

$$L_{(p-1)p} = \frac{G_{(p-1)p.123\ldots(p-2)}}{G_{(p-1)(p-1).123\ldots(p-2)}}$$

At this point, we have developed expressions for the optimum frequency response functions in terms of conditioned auto- and cross-spectra; now we need to be able to obtain these spectra from the original nonconditioned spectra. An iterative algorithm was derived by Bendat to do this. (The derivation is lengthy and will be omitted here. Details may be found in reference 3.) The general expression to be used is:

$$G_{ij.123\ldots r} = G_{ij.123\ldots(r-1)} - L_{rj} G_{ir.123\ldots(r-1)} \tag{18}$$

where $i=1,2,3,\ldots p,y$; $j \leq i$; $r < j$

Special cases are

$$r=1: \quad G_{ij.1} = G_{ij} - L_{1j} G_{i1} \qquad i,j = 2,3,\ldots p,y$$

$$r=2: \quad G_{ij.12} = G_{ij.1} - L_{2j} G_{i2.1} \qquad i,j = 3,4,\ldots p,y$$

$$r=3: \quad G_{ij.123} = G_{ij.12} - L_{3j} G_{i3.12} \qquad i,j = 4,5,6,\ldots p,y$$

. . . . . .

$$r=p: \quad G_{yy.123\ldots p} = G_{yy.123\ldots(p-1)} - L_{py} G_{yp.123\ldots(p-1)}$$

To obtain the auto-spectrum form, set i=j in equation (18):

$$G_{jj.123\ldots r} = G_{jj.123\ldots(r-1)} - L_{rj} G_{jr.123\ldots(r-1)} \tag{19}$$

Now rewrite equation (17) with i replaced by r:

$$L_{rj} = \frac{G_{rj.123\ldots(r-1)}}{G_{rr.123\ldots(r-1)}} \tag{20}$$

Take complex conjugates and solve for $G_{jr.123\ldots(r-1)}$, then substitute in equation (19) to obtain

$$G_{jj.123\ldots r} = G_{jj.123\ldots(r-1)} - |L_{rj}|^2 G_{rr.123\ldots(r-1)} \qquad (21)$$

Again, we could evaluate special cases by setting r=1,2,...p and then varying j so that j=r+1, r+2,...p,y. The iterative process of obtaining the ordered conditioned auto-spectra from the original auto-spectra is illustrated in Figure 3.

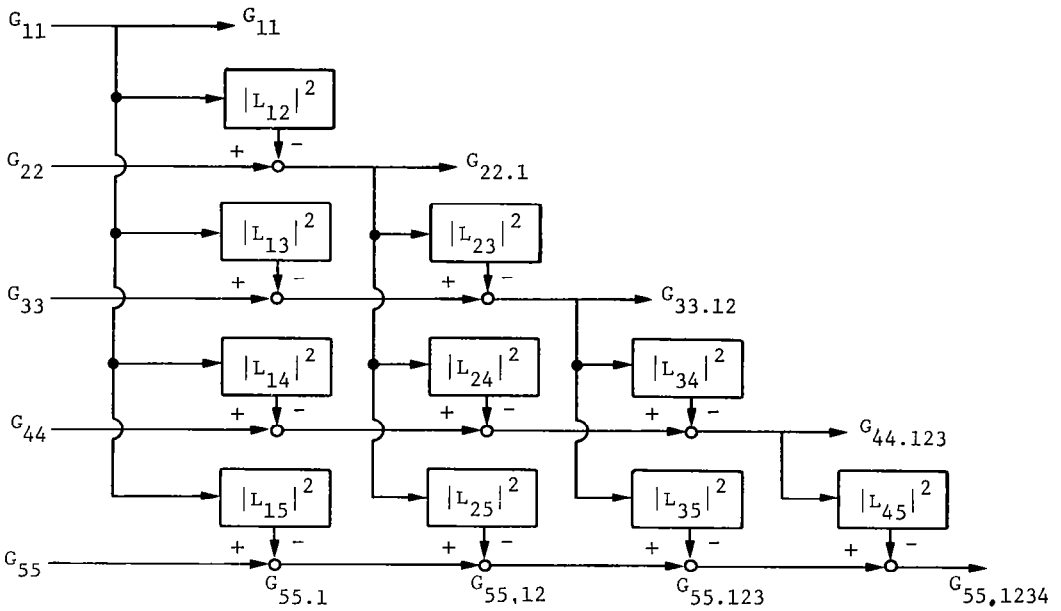

Figure 3. - Diagram showing how ordered conditioned atuo-spectra are obtained from original auto-spectra (from Ref. 3).

From equation (21) it can be proved that, for any r < j where r $\leq$ p,

$$G_{jj} = \sum_{i=1}^{r} |L_{ij}|^2 G_{ii.123\ldots(i-1)} + G_{jj.123\ldots r} \qquad (22)$$

Now if we set r=p and let j=y, equation (22) yields a form similar to equation (6):

$$G_{jj} = \sum_{i=1}^{r} |L_{iy}|^2 G_{ii.123\ldots(i-1)} + G_{nn} \qquad (23)$$

The PCF between the conditioned inputs and outputs are now defined as

$$\gamma^2_{iy.123\ldots(i-1)} = \frac{\left|G_{iy.123\ldots(i-1)}\right|^2}{G_{ii.123\ldots(i-1)}\, G_{yy.123\ldots(i-1)}} \tag{24}$$

A general formula connecting multiple coherence functions with associated ordinary and partial coherence functions is derived in reference 7. For a system with p inputs, this formula is

$$\gamma^2_{y:x} = 1 - \{(1-\gamma^2_{1y})(1-\gamma^2_{2y.1})(1-\gamma^2_{3y.12})\ldots.(1-\gamma^2_{py.123\ldots(p-1)})\} \tag{25}$$

Note that $\gamma^2_{y:x} = 1$ if and only if <u>one</u> of the OCF and PCFs equals unity, and $\gamma^2_{y:x} = 0$ if and only if <u>all</u> of these functions equal zero. For the case where the inputs are independent, equation (25) reduces to the simpler result in equation (11).

ANALYSIS OF THREE INPUT/SINGLE OUTPUT SYSTEM

The general theory discussed in the previous section was applied to the special case of a system with three inputs, which may either be independent or mutually coherent, and a single output. This system corresponds to the test setup used to obtain data from which the computational technique was developed.

The test results provided inputs $x_1(t)$, $x_2(t)$, $x_3(t)$ and an output $y(t)$; both independent and coherent inputs were applied as separate cases. These time histories were then processed to yield averaged estimates of auto-spectra $G_{11}(f)$, $G_{22}(f)$, $G_{33}(f)$ and $G_{yy}(f)$ and (for the coherent case) cross-spectra $G_{12}(f)$, $G_{13}(f)$, $G_{1y}(f)$, $G_{23}(f)$, $G_{2y}(f)$ and $G_{3y}(f)$. For the independent input case, the OCFs were computed using equations (7) and (8), and then the MCF calculated from equation (11). This was the extent of the computations performed for the independent input case. In the coherent input case, the OCFs were computed for use in reordering the inputs. The ordered, conditioned auto- and cross-spectra were next calculated from equations (18) and (19). To start the iterative computation process, it is necessary to calculate the first set of optimized frequency response functions from equation (17):

$$L_{12} = \frac{G_{12}}{G_{11}} \qquad L_{13} = \frac{G_{13}}{G_{11}} \qquad L_{1y} = \frac{G_{1y}}{G_{11}} \tag{26}$$

- note that these are ratios of nonconditioned spectra only.

The relationships in equations (18), (21), and (26) allow us to calculate the following:

$$\left.\begin{aligned} G_{22.1} &= G_{22} - |L_{12}|^2 G_{11} \\ G_{33.1} &= G_{33} - |L_{13}|^2 G_{11} \\ G_{yy.1} &= G_{yy} - |L_{1y}|^2 G_{11} \end{aligned}\right\} \tag{27}$$

$$\left.\begin{aligned} G_{23.1} &= G_{23} - L_{13}\, G^*_{12} \\ G_{2y.1} &= G_{2y} - L_{1y}\, G^*_{12} \\ G_{3y.1} &= G_{3y} - L_{1y}\, G^*_{13} \end{aligned}\right\} \tag{28}$$

The next set of frequency response functions can now be calculated:

$$L_{23} = \frac{G_{23.1}}{G_{22.1}} \qquad L_{2y} = \frac{G_{2y.1}}{G_{22.1}} \tag{29}$$

Knowing these, we can compute

$$\left.\begin{aligned} G_{33.12} &= G_{33.1} - |L_{23}|^2 G_{22.1} \\ G_{yy.12} &= G_{2y.1} - |L_{2y}|^2 G_{22.1} \\ G_{3y.12} &= G_{3y.1} - L_{2y} G_{23.1}^{*} \end{aligned}\right\} \tag{30}$$

Next,

$$L_{3y} = \frac{G_{3y.12}}{G_{33.12}} \tag{31}$$

Finally, the auto-spectrum of the noise at the output may be calculated:

$$\begin{aligned} G_{yy.123} &= G_{nn} \\ &= G_{yy} - |L_{1y}|^2 G_{11} - |L_{2y}|^2 G_{22.1} - |L_{3y}|^2 G_{33.12} \end{aligned} \tag{32}$$

Using equations (27), (28), and (30), the two partial coherence functions may be calculated:

$$\gamma^2_{2y.1} = \frac{|G_{2y.1}|^2}{G_{22.1}\, G_{yy.12}} \tag{33}$$

$$\gamma^2_{3y.12} = \frac{|G_{3y.12}|^2}{G_{33.12}\, G_{yy.12}} \tag{34}$$

The multiple coherence function is given by

$$\gamma^2_{y:x} = 1-(1-\gamma^2_{1y})(1-\gamma^2_{2y.1})(1-\gamma^2_{3y.12}) \tag{35}$$

The computational process is summarized in the flow chart.

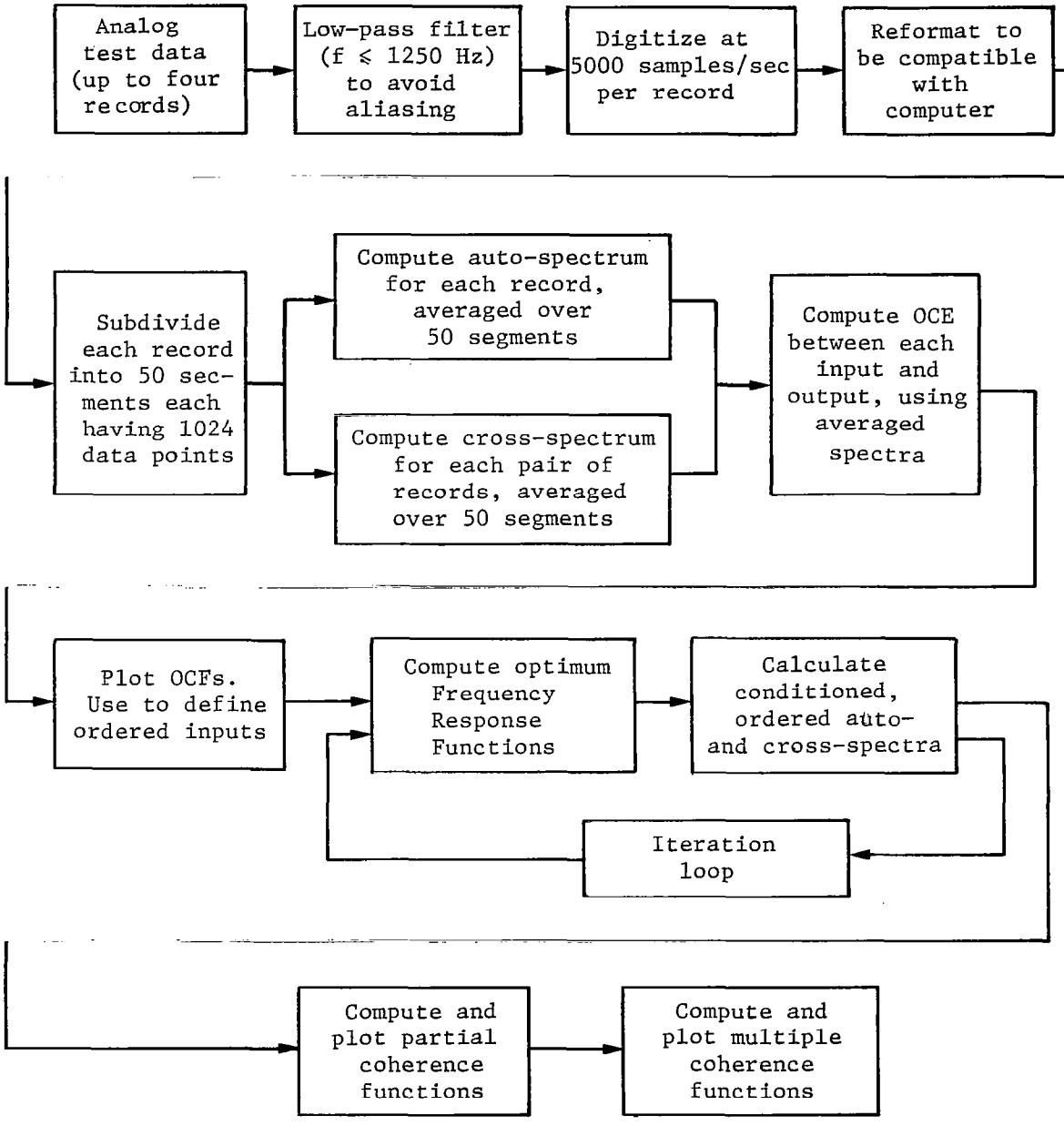

Figure 4. - Flow chart showing computation of coherence functions.

EXPERIMENTAL PROGRAM

Testing was performed on a typical aerospace structure to provide data for use in demonstrating the computational technique. The structure was an instrument support truss from a Titan launch vehicle, shown in Figure 5. A panel, carrying a simulated component, was mounted on the top of the truss (see Fig. 6). It was designed so that its first three resonances would occur in the range 50 to 200 Hz. The assembly was supported inside the Martin Marietta acoustic chamber on a 2 Hz suspension system and was connected via two push rods to two electromagnetic shakers. The shakers were mounted on rubber isolation pads to minimize feedback of mechanical vibration through the floor.

The test setup was designed to allow application of two separate random mechanical vibration inputs through the truss to the panel, combined with direct acoustically-induced vibration. Thus, as many as three inputs could be applied simultaneously. The output was defined as the response measured at the simulated component on the panel.

The test program was conducted in two phases. In Phase I, all of the inputs were stationary; that is, their statistical properties were time invariant. All of the theoretical developments discussed earlier are based on the assumption of stationarity. In Phase II, the inputs were deliberately made nonstationary so that, strictly speaking, the definitions of the various coherence functions were no longer valid. The data provided by Phase II were required so that the errors introduced by falsely assuming stationarity could be evaluated for a particular case.

Table 1 lists the test runs that were performed in Phase I showing the various input conditions. For the "coherent input" case, the two shakers were driven through a single power amplifier/random noise generator system. For the case of three independent inputs, separate power amplifiers and random noise generators were used.

Table 2 shows the inputs used for the Phase II test. Only two inputs were used, consisting of mechanical vibration from one shaker combined with acoustics. It was considered that this setup was sufficiently complicated, in view of the additional complexity introduced by the lack of stationarity.

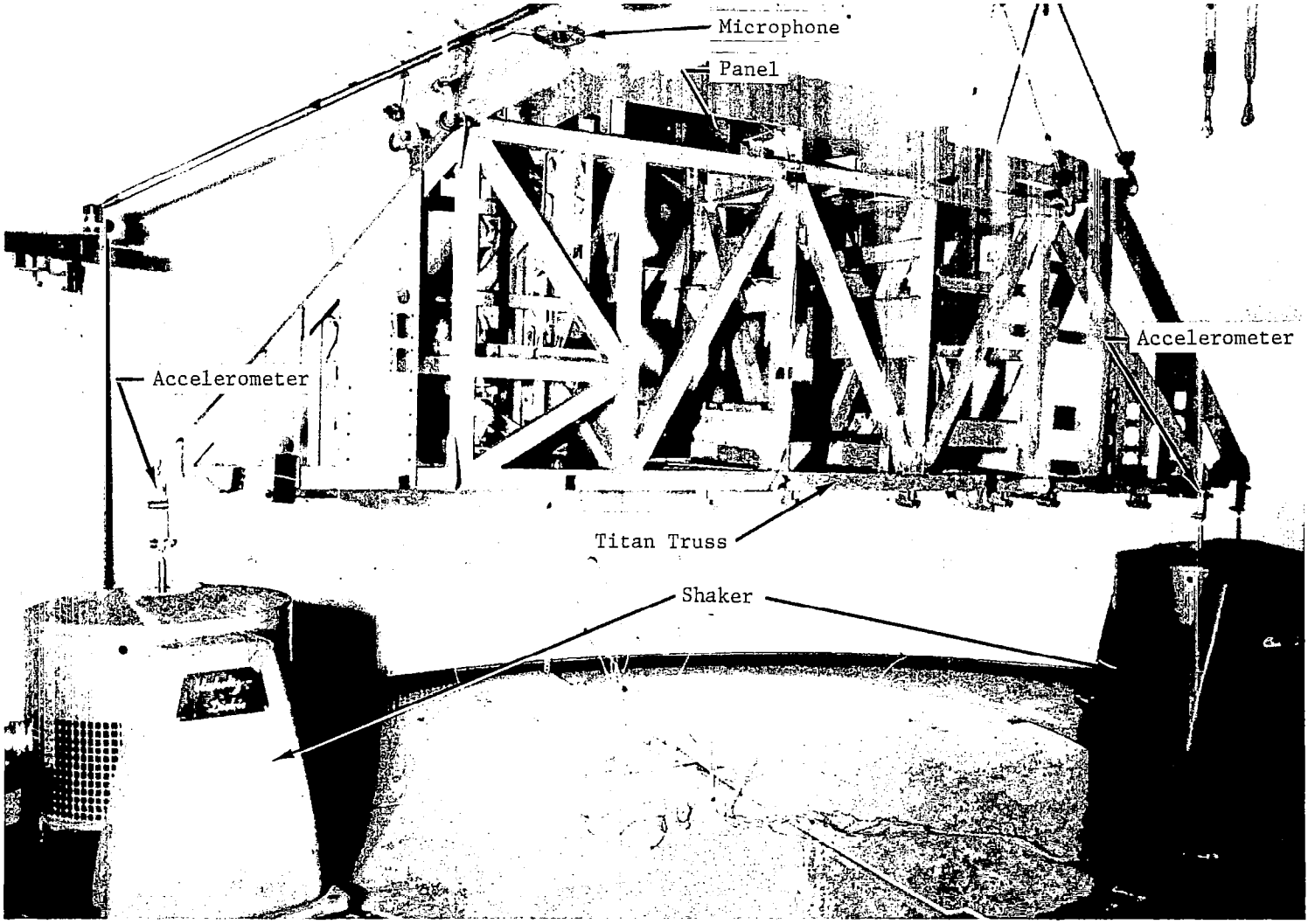

Figure 5. - Test setup.

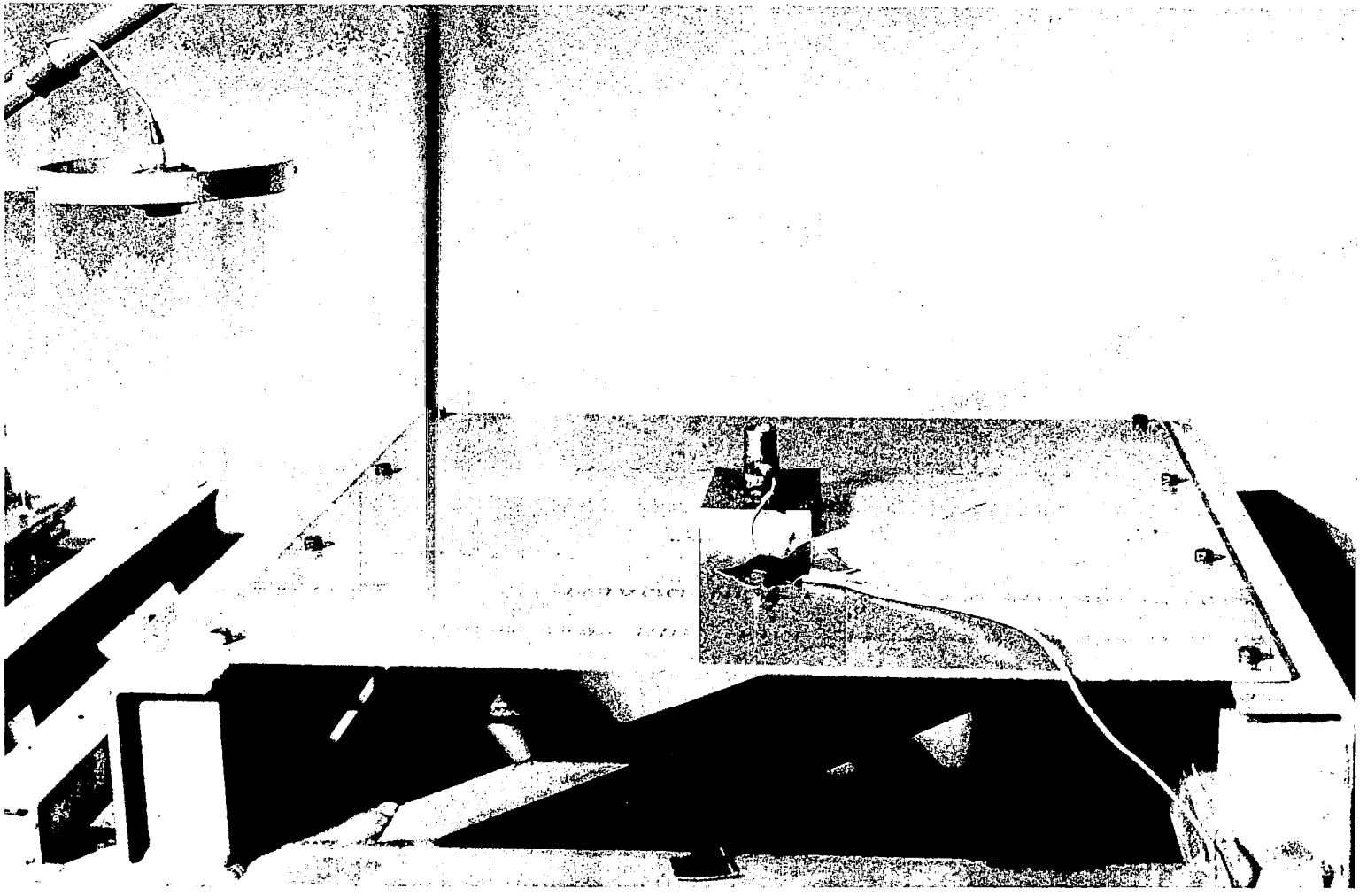

Figure 6. - Close-up of panel, showing response accelerometer and microphone.

TABLE 1. - PHASE I TEST RUNS

Run No.	Input Conditions			Notes
	Shaker 1	Shaker 2	Acoustics	
1	X	X		Shakers coherent
2	X	X	X	Shakers coherent, acoustics indept.
3	X	X	X	Indept. inputs
4	X			
5			X	
6	X		X	Indept. inputs

TABLE 2. - PHASE II TEST RUN

Run No.	Input Conditions
7	a) Acoustic spectrum same shape as in run no. 6, with overall sound pressure level varying as follows: 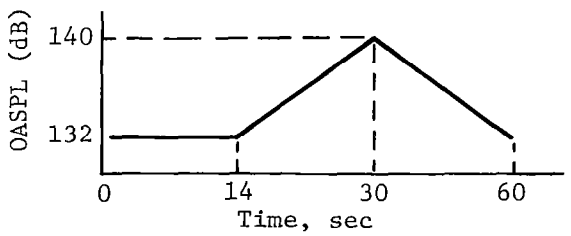 b) Vibration spectrum same shape as run no. 6, with RMS acceleration level varying as follows: 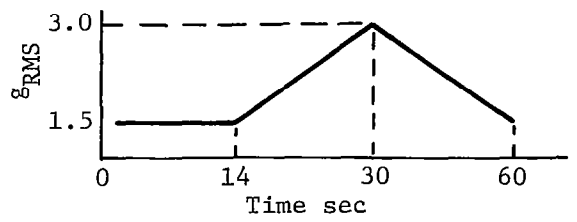

The transducers used to measure the inputs and the outputs are identified in the notation used for the data analysis, in Figure 7.

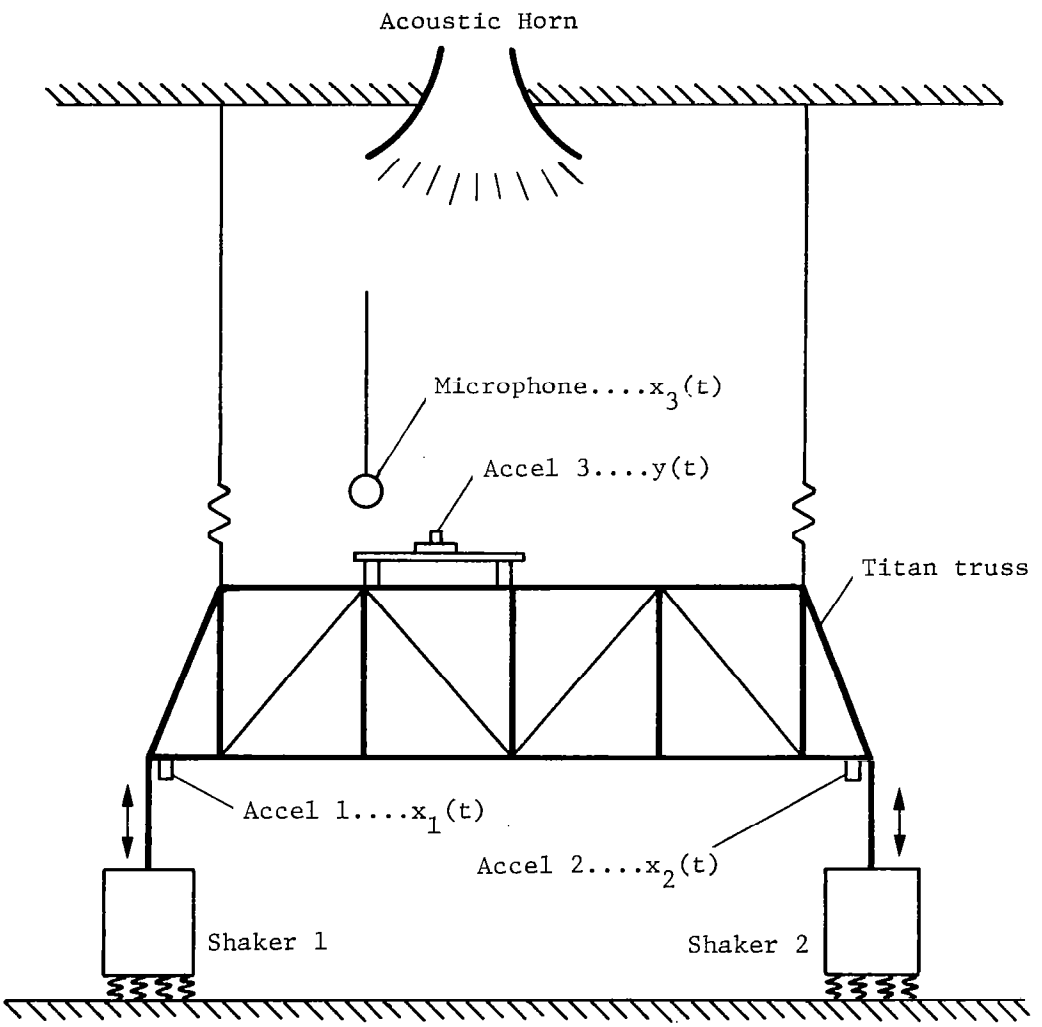

Figure 7. - Sketch of test setup.

DISCUSSION OF RESULTS

Phase I: Stationary Inputs

Checks were first performed to verify that the digitized data were correctly scaled. The time history from one of the accelerometer channels was played back on an oscillograph record directly from the analog tape and compared with the corresponding digitized time history. Next, the acceleration spectral density was plotted using an analog data analysis system and compared with the acceleration spectral density obtained from the digitized time history using a Fast Fourier Transform (FFT) method. Finally, a one-third octave band Sound Pressure Level spectrum was plotted from a sample of the analog microphone data and used to calculate the corresponding Pressure Spectral Density plot; this was then compared with the same plot resulting from the digital analysis. The three comparisons confirmed that the scaling used in the analog-digital conversion and the subroutines written to calculate the spectra were correct.

The technique used on the test data consisted of first calculating the auto- and cross-spectra for the inputs and output signals, averaged over 50 segments of data, then computing the OCF between each pair of inputs (γ^2_{ij}) and between each input-output combination (γ^2_{iy}). The γ^2_{ij} were then reviewed to determine whether the two inputs x_i and x_j should be treated as being independent or correlated (i.e., mutually coherent). According to Bendat (Ref. 8), a value of γ^2_{ij} of 0.1 is low enough for an assumption of independence; a higher value indicates significant coherence between the inputs. At the other end of the scale, $\gamma^2_{ij} \geq 0.9$ means that the two inputs are effectively fully coherent and should therefore be treated as a single input to the system.

For the runs in which the inputs were judged to be independent, the MCF between the total set of inputs and the output was then computed by adding up the γ^2_{iy}, as indicated by equation (11). For the tests involving coherent inputs, the γ^2_{iy} were used to reorder the inputs (if necessary) as discussed earlier and then PCFs and the MCF were computed, using equations (26) through (35). The results of treating the data by these techniques will now be discussed for each test run.

Run 1 (two shakers, correlated). - Acceleration spectral density plots for the two inputs and the response are presented in Figure 8. The inputs are similar in spectrum shape at both shakers, and reflect the resonances and antiresonances of the truss structure. The response of the panel is shown to occur as prominent peaks at approximately 68 Hz, 161 Hz, 230 Hz and 410 Hz, with many intermidiate minor peaks.

Coherence function plots are given in Figures 9 through 11. Figure 9 is the OCF between the two inputs. It shows that the two inputs were well correlated; in fact, by Bendat's criterion, their mutual coherence was high enough (>0.90) over much of the frequency range that the system should be regarded as having only a single input. On this basis, the OCF between either input and the response should be essentially the same, and should theoretically be unity across the frequency band if the system were linear and noise-free. A comparison of Figures 10 and 11 shows that they are very similar; however, neither OCF ever reaches unity, indicating the existence of nonlinearities and/or measurement noise in the system.

Run 2 (two shakers, correlated, plus acoustics). - Acceleration and pressure spectral density plots for the three inputs and the response are given in Figure 12. The shaker inputs were again very similar in spectrum shape and the response peaks occurred at approximately the same frequencies as in Run 1.

The OCF between the two shaker inputs is plotted in Figure 13. This shows that the coherence between the inputs was considerably less than for Run 1, particularly in the frequency range below 100 Hz. However, the OCF was in the desired range of 0.10 to 0.90 over most of the frequency band. The OCFs between each individual shaker input and the acoustics input were examined next; these are presented in Figures 14 and 15. Although the shaker inputs and the acoustic inputs were theoretically independent, a significant degree of mutual coherence is indicated. This is thought to be caused by the acoustically induced panel response being transmitted through the truss structure and coupled into the vibration environment as recorded by the shaker input accelerometers. The Run 2 data were therefore treated as representing a system with three correlated inputs and a single output.

The resulting coherence functions are shown in Figures 16 through 20. When these are examined in conjunction with the panel response plot [Figure 12(d)], several features become apparent:

(1) Figure 16 indicates $\gamma^2_{iy} = 0.78$ at 68 Hz, showing that the high response at this frequency resulted mainly from the shaker 1 input. Figures 17 and 18 are plots of the Partial Coherence

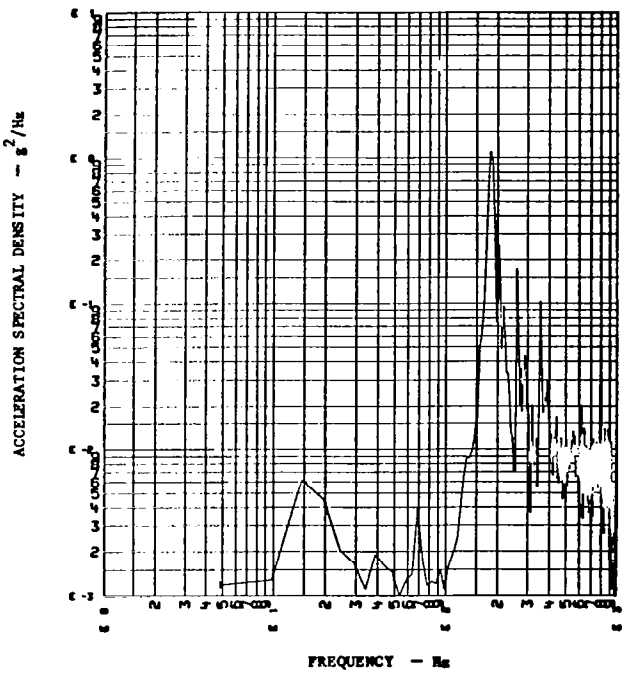

(a) Shaker 1 input

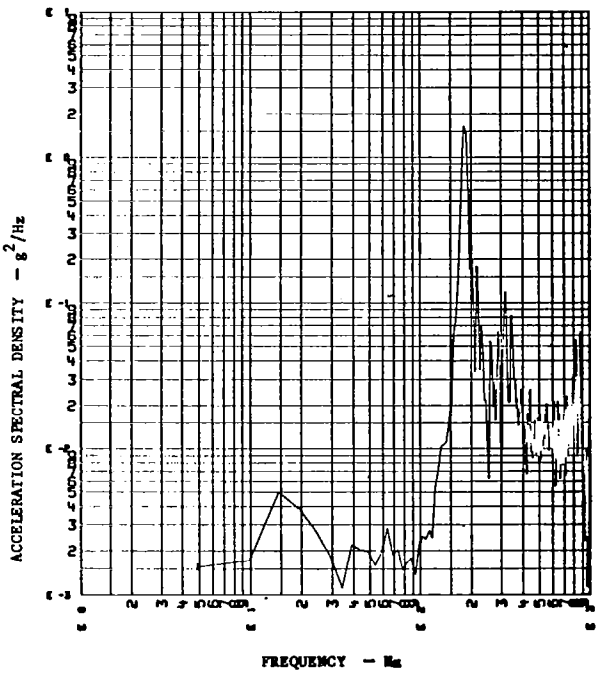

(b) Shaker 2 input

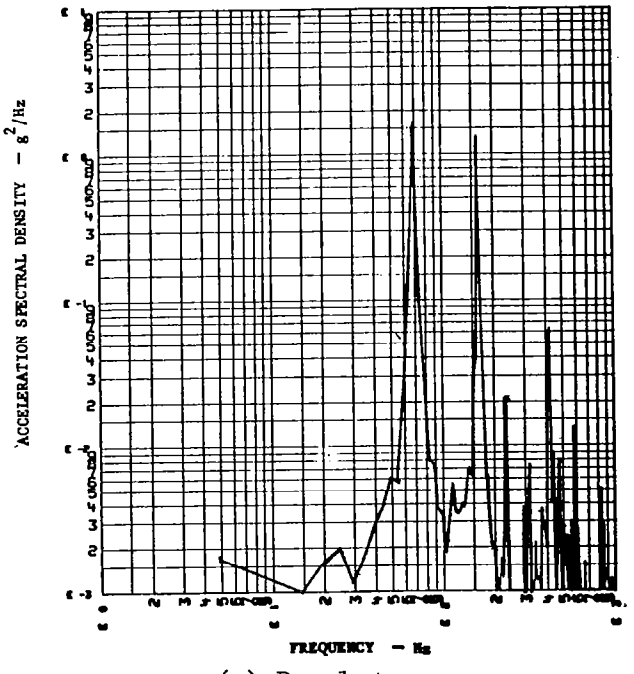

(c) Panel response

Figure 8: Input and response data for run 1

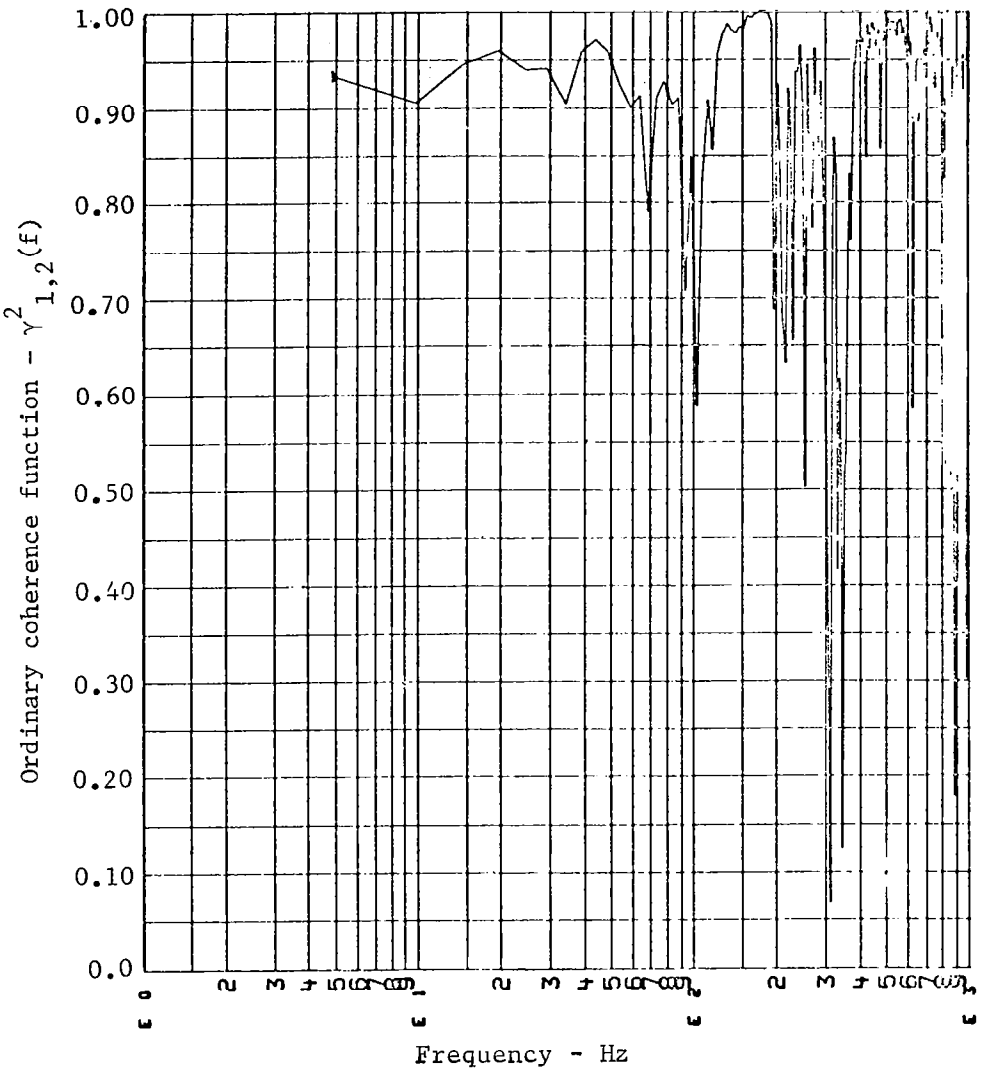

Figure 9: Ordinary coherence function between shaker #1 and shaker #2 inputs (run 1)

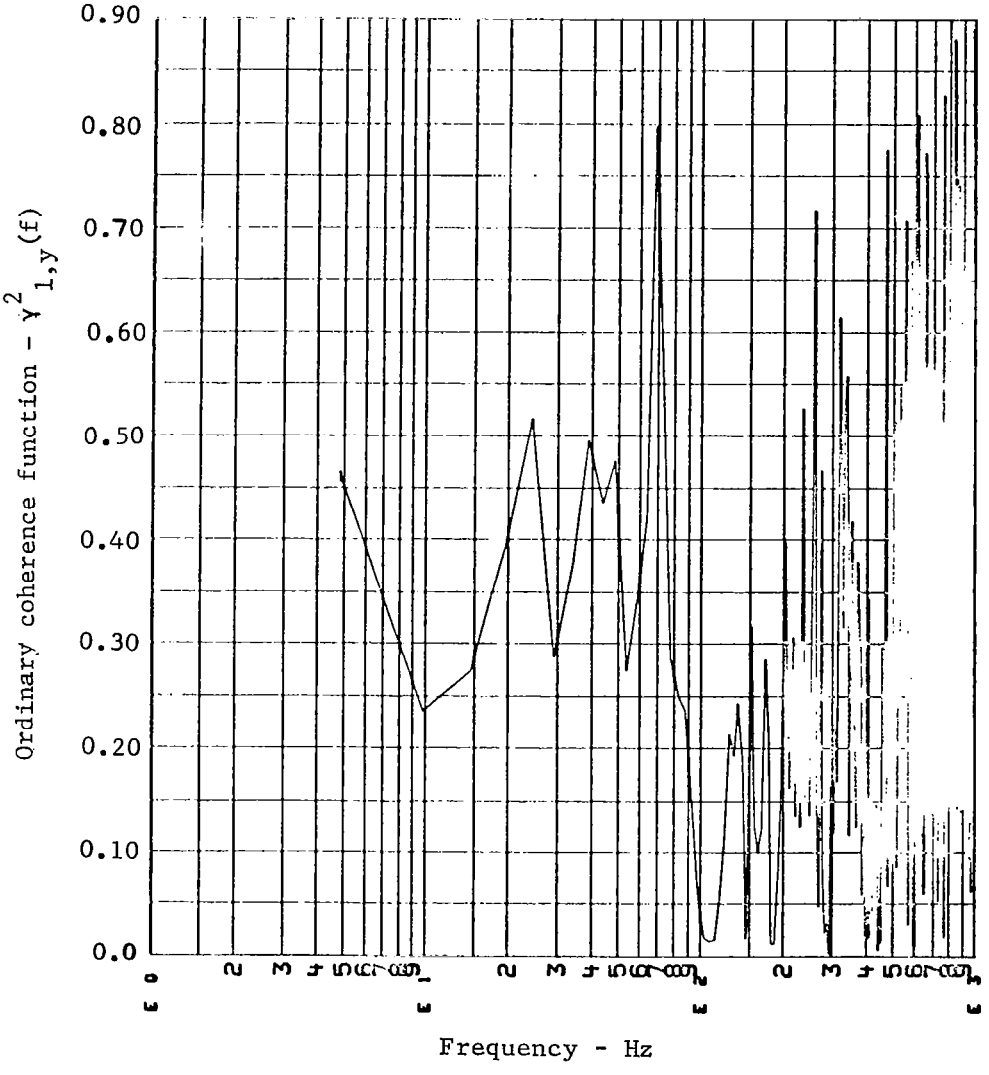

Figure 10. - Ordinary coherence function between shaker 1 input and panel response (run 1)

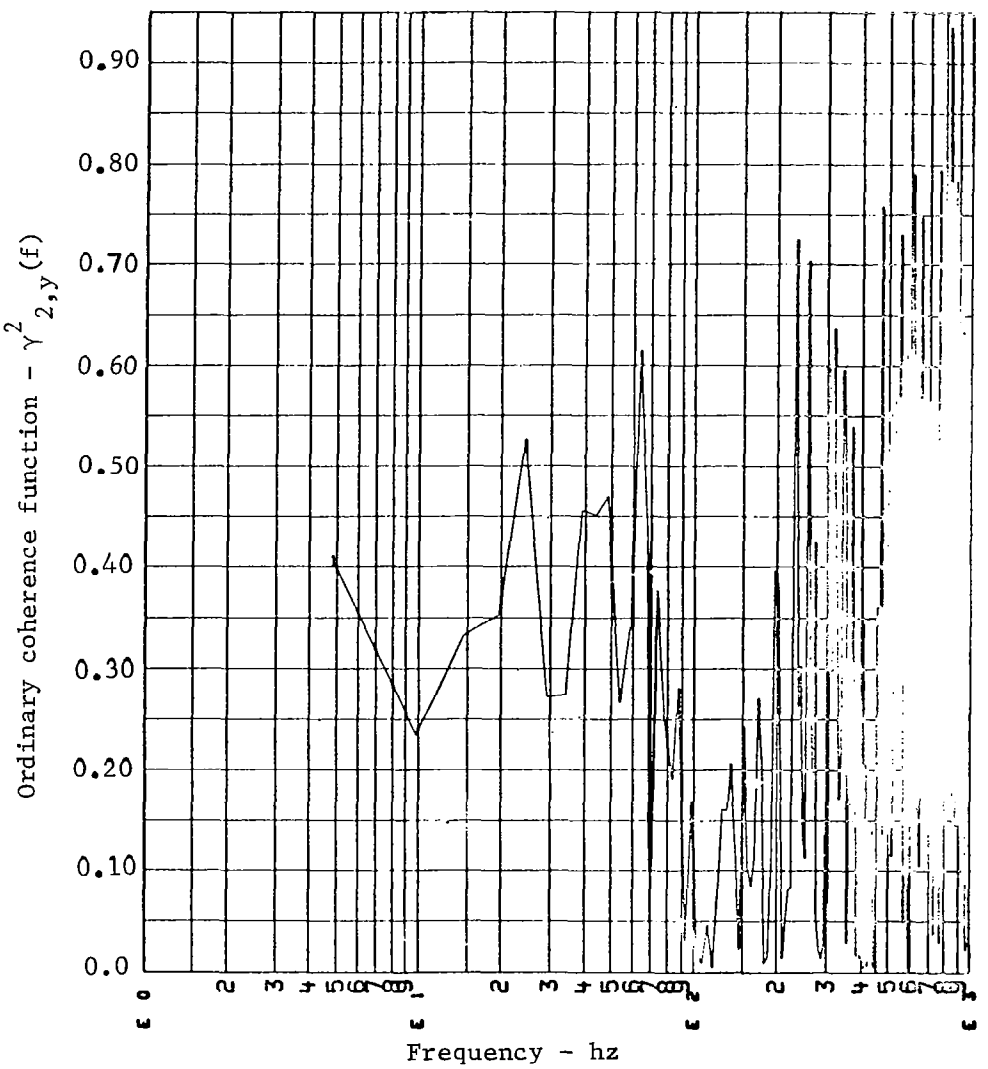

Figure 11. - Ordinary coherence function between shaker 2 input and panel response (run 1)

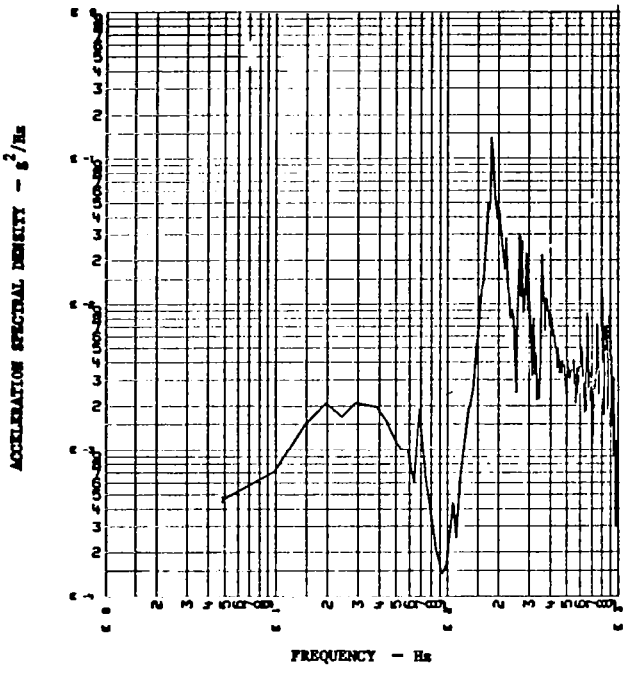

(a) Shaker 1 input

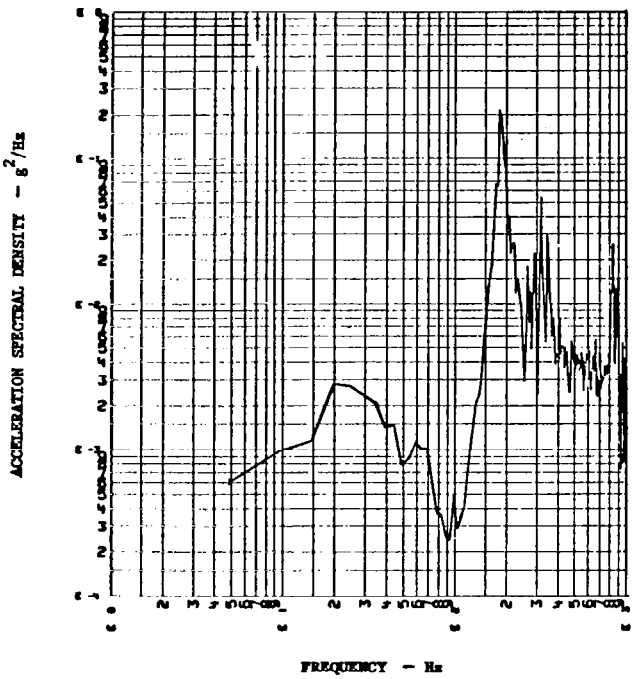

(b) Shaker 2 input

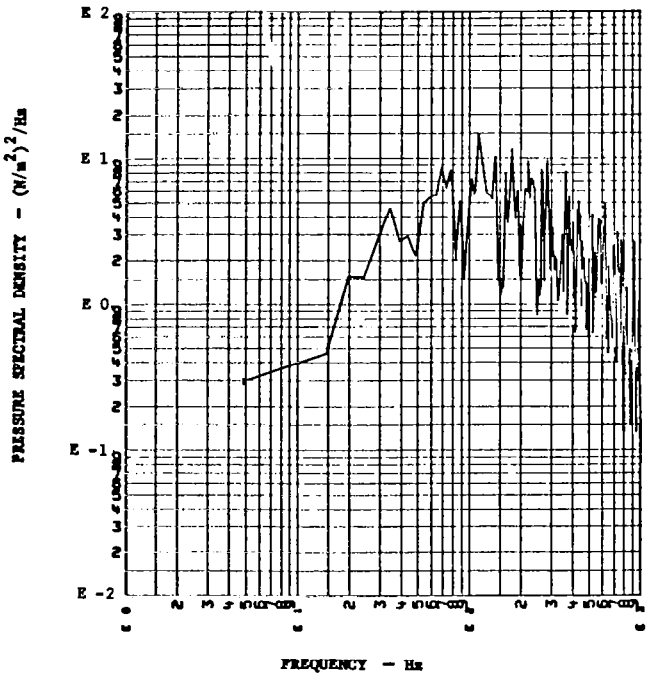

(c) Acoustic input

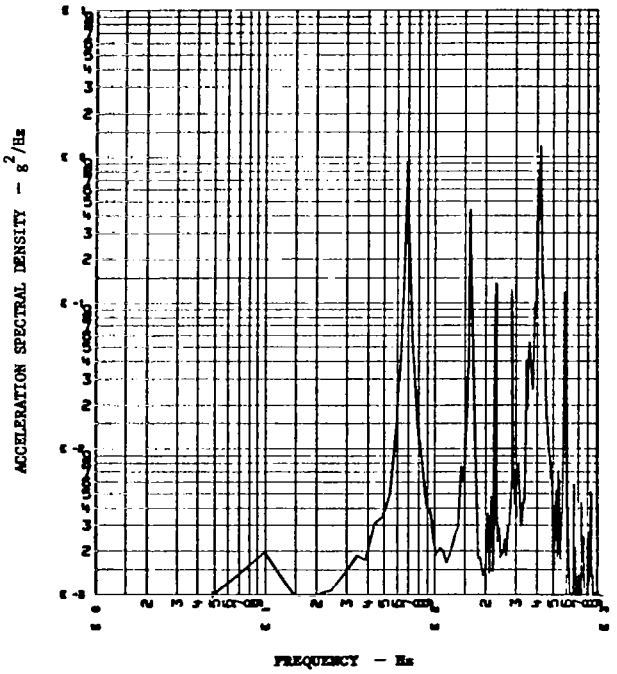

(d) Panel response

Figure 12. - Input and response data for run 2

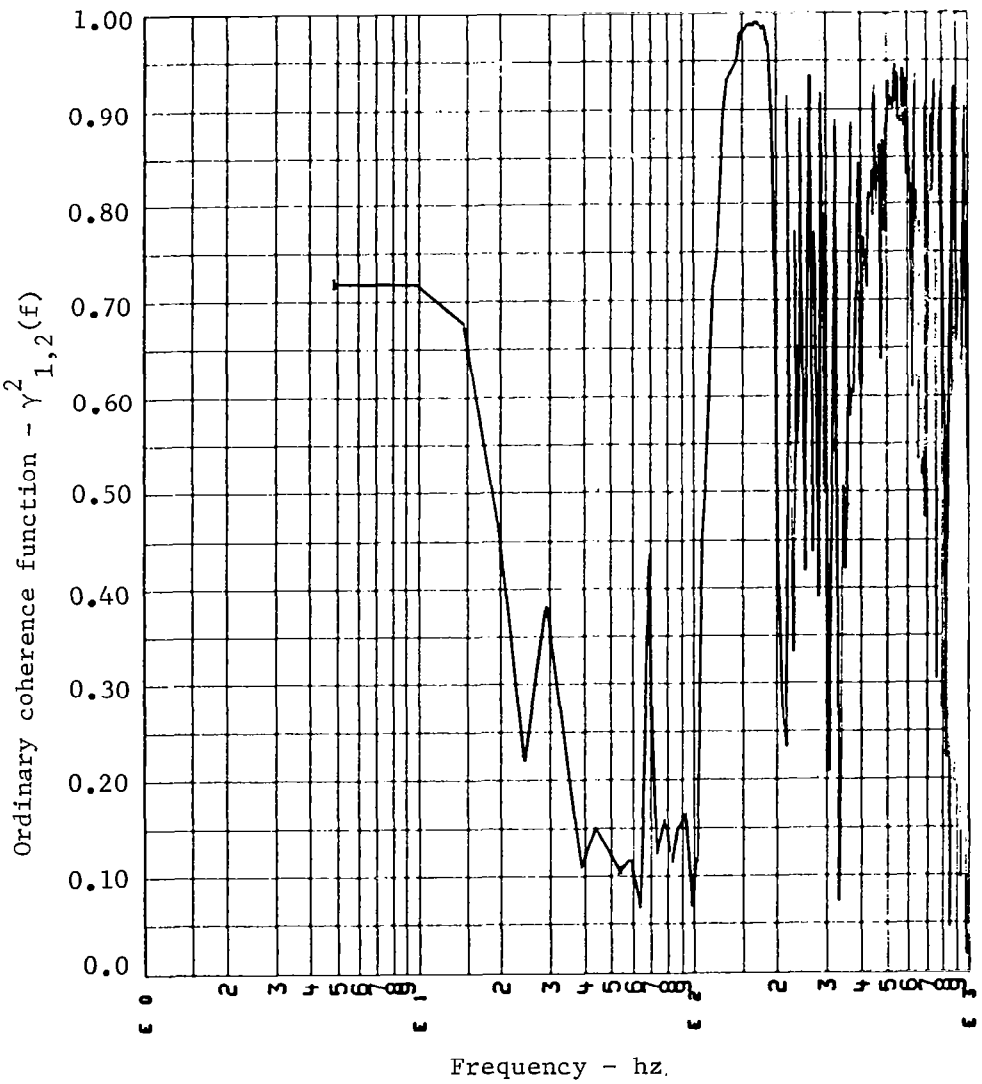

Figure 13. - Ordinary coherence function between shaker 1 and shaker 2 inputs (run 2)

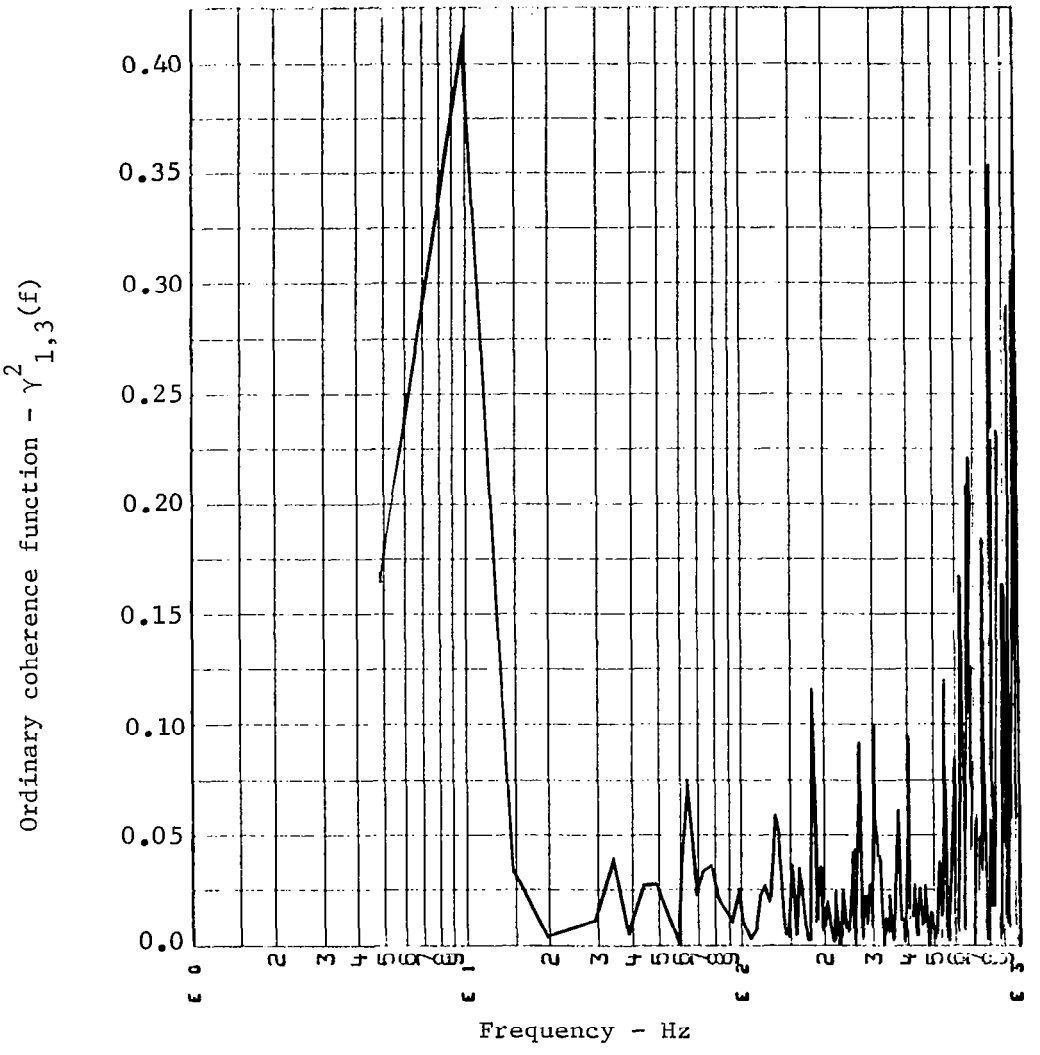

Figure 14. - Ordinary coherence function between shaker 1 and acoustics (run 2)

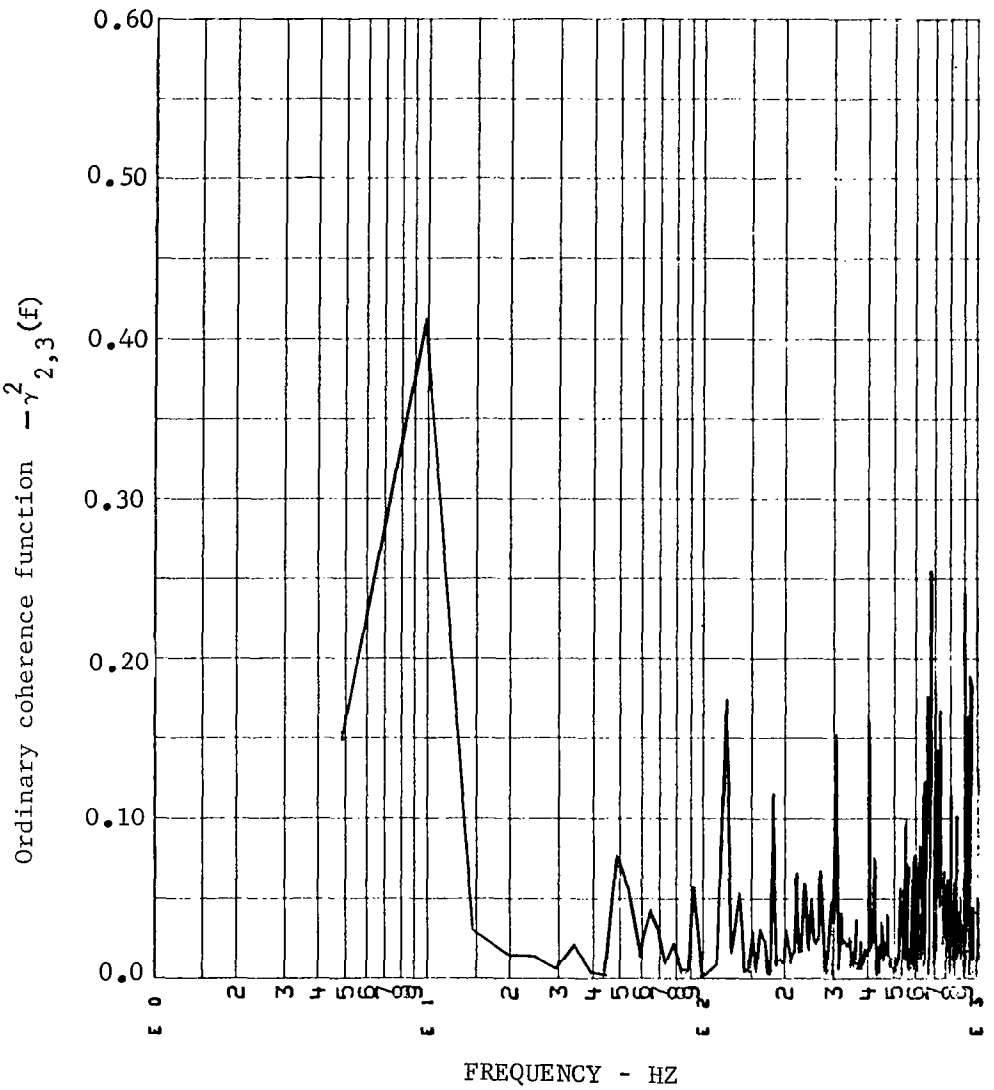

Figure 15 - Ordinary coherence function between shaker #2 and acoustics (Run 2)

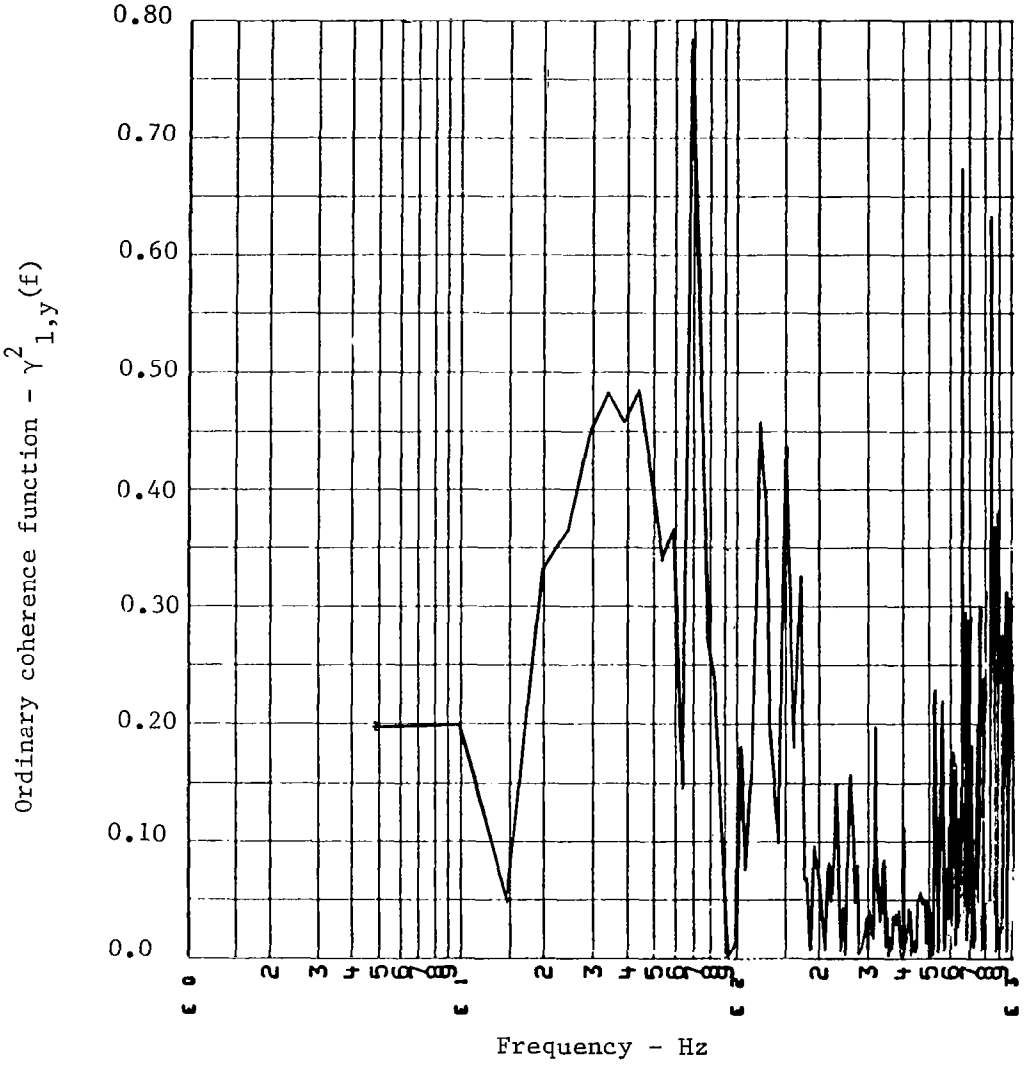

Figure 16. - Ordinary coherence function between shaker 1 input and panel response (run 2).

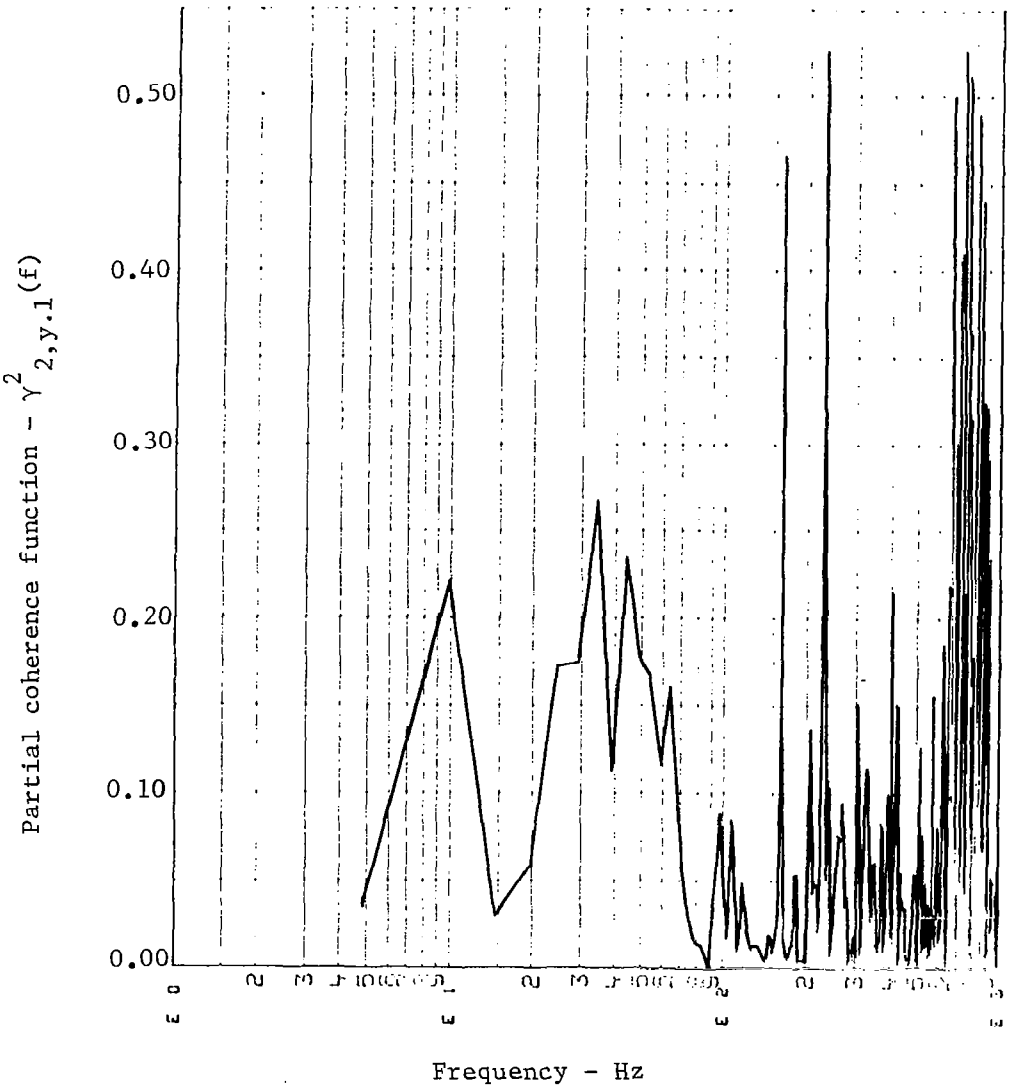

Figure 17. - Partial coherence function between shaker 2 input and panel response (run 2).

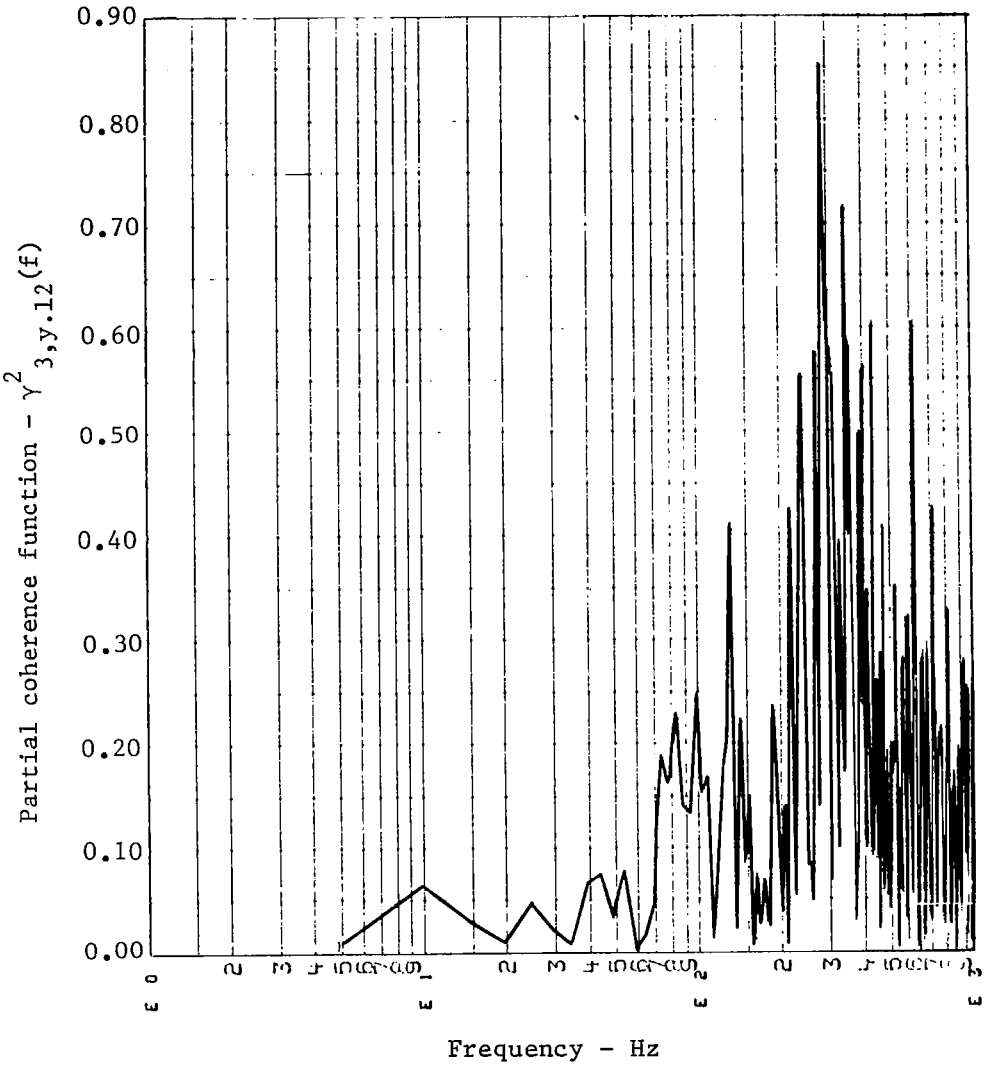

Figure 18. - Partial coherence function between acoustic input and panel response (run 2).

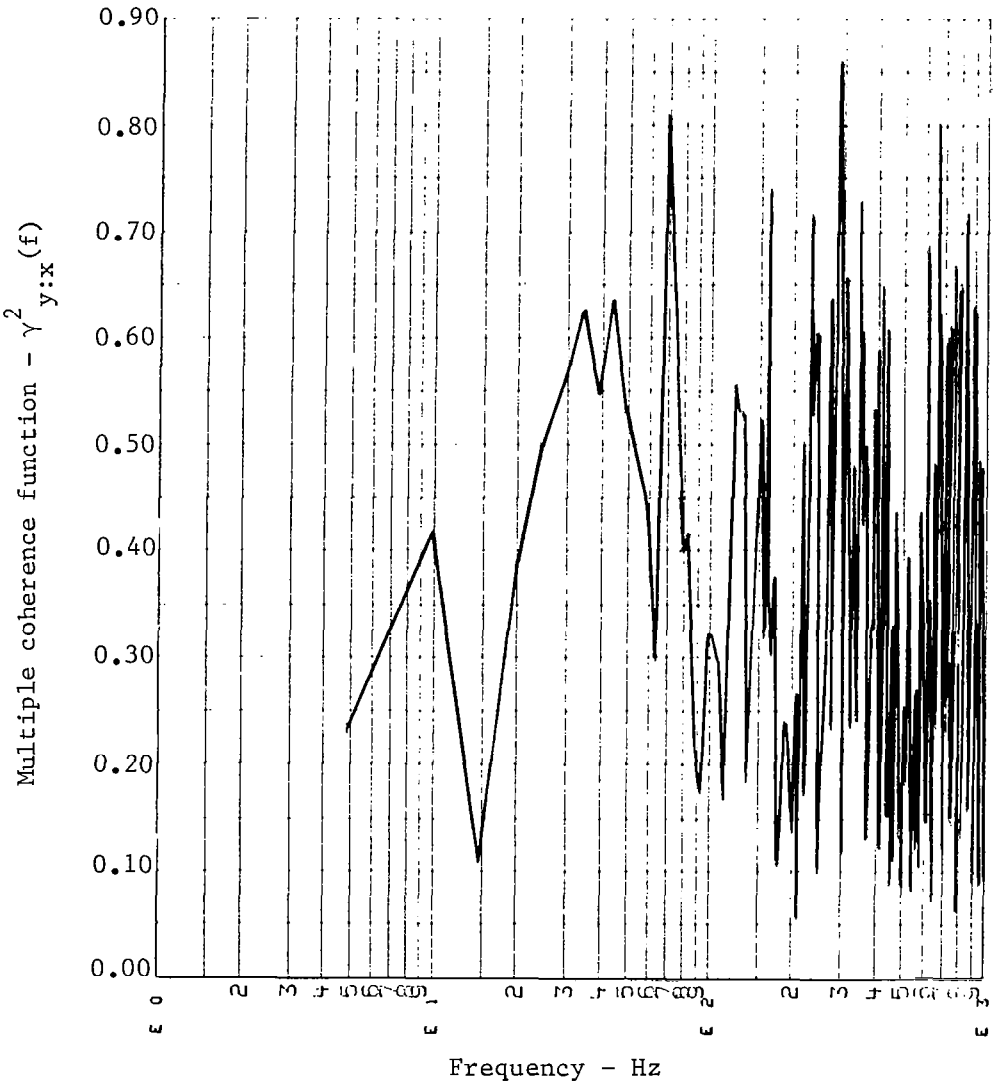

Figure 19. - Multiple coherence function between total set of inputs and panel response (run 2).

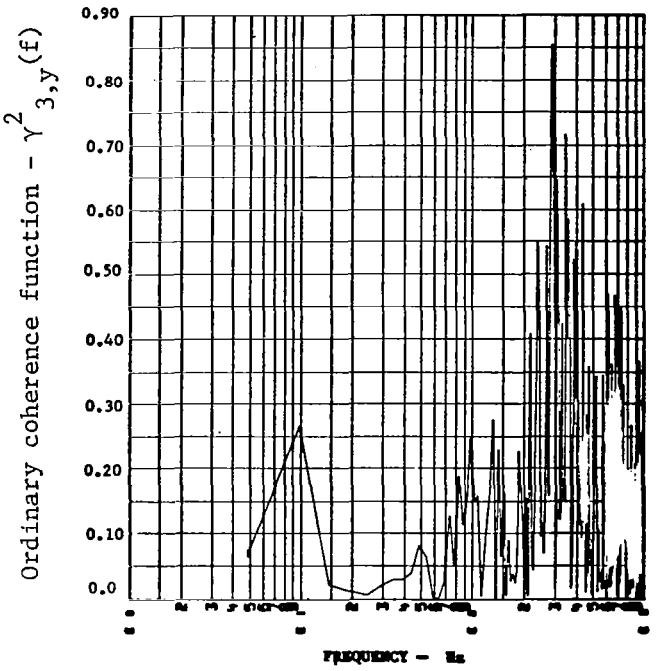

(a) Ordinary coherence function

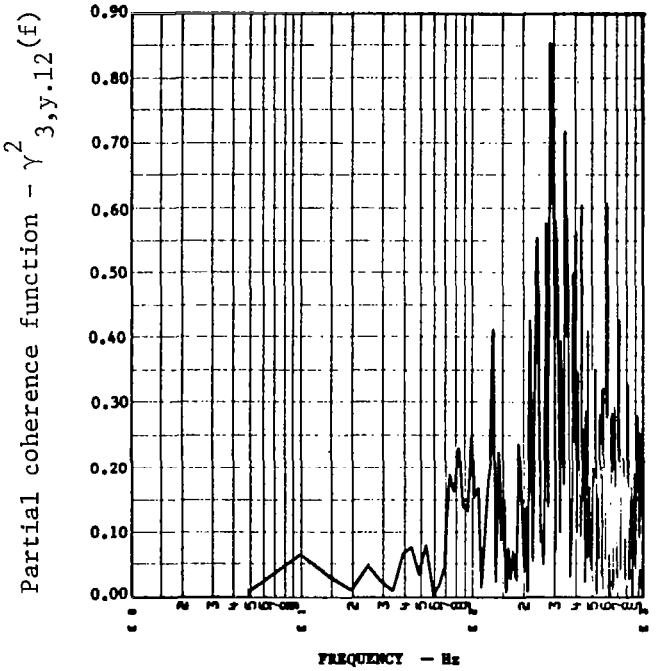

(b) partial coherence function

Figure 20. - Comparison of ordinary and partial coherence functions between acoustic input and panel response, for run 2.

Functions (PCF) between shaker 2 and panel response with the effects of shaker 1 removed, and between the acoustic input and panel response with the effects of both shakers removed. Both PCFs have low values at 68 Hz, indicating little contribution to the response.

(2) The next response peak is at approximately 160 Hz. Figure 16, 17, and 18 show that the two shakers were primarily responsible for this peak, having OCF and PCF values of 0.44 and 0.47 respectively. The PCF associated with the acoustic input at this frequency is less than 0.10. It is interesting to note that, from Figure 13, the mutual coherence between the two shakers was very high (≈ 0.98) in the 150-180 Hz. range, whereas the mutual coherences between the individual shakers and the acoustic input (Figures 14 and 15) were close to zero (≈ 0.02). Thus, in this frequency band, the system should actually be analyzed as a model having two independent inputs and a single output.

(3) The third response peak, occurring at about 230 Hz, was due mainly to the input from shaker 2, since $\gamma^2_{2y.1} = 0.53$, whereas $\gamma^2_{1y} = 0.15$ and $\gamma^2_{3y.12} = 0.26$ at this frequency.

(4) Another narrow response peak is seen at approximately 290 Hz. The CF values at 290 Hz are $\gamma^2_{1y} = 0.02$, $\gamma^2_{2y.1} = 0.01$ and $\gamma^2_{3y.12} = 0.85$; thus, this peak was clearly caused by the acoustic input.

(5) A rather broad response peak is centered at about 420 Hz. This also appears to have been caused by the acoustic input, which has $\gamma^2_{3y.12} = 0.6$. The OCF and PCF for the shakers are approximately $\gamma^2_{1y} = 0.05$ and $\gamma^2_{2y.1} = 0.06$.

The following table3 summarizes the ordinary and partial coherence functions associated with the first six response peaks on the panel. The multiple coherence function values (taken from Fig. 19) at these frequencies are also tabulated and compared with the sum of the three individual coherence functions.

The sum of the individual coherence functions is close to unity in every case, and is higher than the MCF at all of the modal frequencies. It can easily be shown that $\Sigma\gamma^2$ will always exceed $\gamma^2_{y:x}$, as follows:

From equation (35), $\gamma^2_{y:x} = 1 - (1 - \gamma^2_{1y})(1 - \gamma^2_{2y.1})(1 - \gamma^2_{3y.12})$ for a three input system. For brevity, write this as

TABLE 3. - VALUES OF COHERENCE FUNCTIONS AT PANEL RESONANCES (RUN 2).

Frequency, Hz	γ^2_{1y}	$\gamma^2_{2y.1}$	$\gamma^2_{3y.12}$	$\Sigma\gamma^2$	$\gamma^2_{y:x}$
68	0.78	0.09	0.04	0.91	0.81
161	0.44	0.47	0.08	0.99	0.73
230	0.15	0.56	0.26	0.97	0.72
290	0.02	0.01	0.85	0.88	0.86
420	0.05	0.06	0.60	0.71	0.64
600	0.12	0.07	0.60	0.79	0.68

$$\gamma^2_{y:x} = 1 - (1 - A)(1 - B)(1 - C)$$
$$= 1 - (1 - A - B - C + AB + BC + CA - ABC)$$
$$= (A + B + C) - (AB + BC + CA) + ABC \quad (36)$$

In the same notation, $\Sigma\gamma^2 = A + B + C$ (37)

$$\therefore \Sigma\gamma^2 - \gamma^2_{y:x} = (AB + BC + CA) - ABC$$
$$= AB\ (1 - C) + BC + CA \quad (38)$$

Since $\{A, B, C\} \leq 1.0$, the quantity $(1 - C)$ is always positive or zero, so that $\Sigma\gamma^2$ must always be greater than the multiple coherence function $\gamma^2_{y:x}$.

The amount by which the MCF is less than one represents the effects of noise and nonlinearities in the system. Since these effects may be assumed to be statistically independent of the inputs they do not contaminate the individual coherence functions associated with the inputs, only the multiple coherence function, which represents the coherence between the full set of inputs and the measured output.

As a final comment, Figure 20 allows a direct comparison of the PCF between the acoustic input and the panel response ($\gamma^2_{3y.12}$, Fig. 18) with the OCF that is obtained when the mutual coherence between the acoustic input and the shaker inputs is neglected. It can be seen that the difference between the two CFs is very small, implying that the errors introduced by the simplified approach would be negligible in this particular case.

Run 3 (two shakers, noncorrelated, plus acoustics). - The input and response data are plotted in Figure 21. It was intended to use shaker inputs that were uncorrelated with each other as well as with the acoustic input, giving three independent inputs. However, when the OCF between the two shakers was plotted (Fig. 22), it was found that high mutual coherence existed at some frequencies between the two measured shaker inputs. This was especially true in the 130-180 Hz region, where a lateral mode exists for the truss, allowing the two shaker input locations to be very closely coupled. To a lesser extent, the acoustic input was found to be coherent with each individual shaker input (Figures 23 and 24); therefore, it was decided to treat the run 3 data as applying to a system with three correlated inputs and a single output, like the run 2 data.

The coherence functions between the three inputs and the output are given in Figures 25 through 28. The plots can be used to identify the contributions of the three excitation sources at

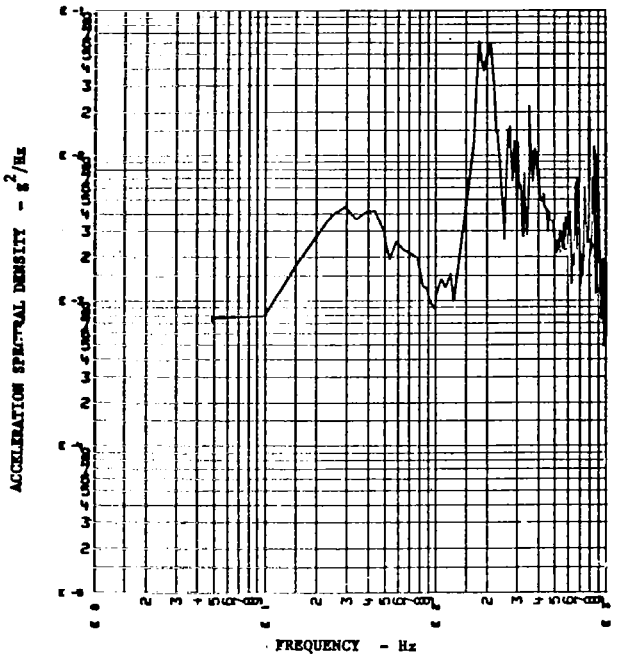

(a) Shaker 1 input

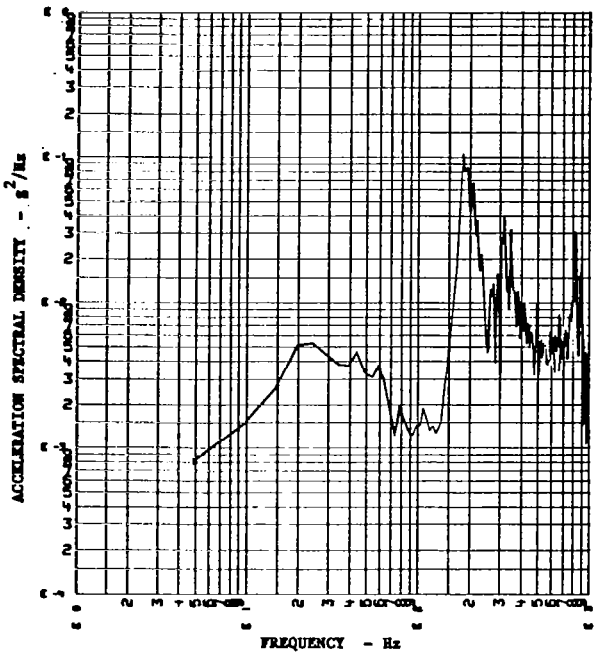

(b) Shaker 2 input

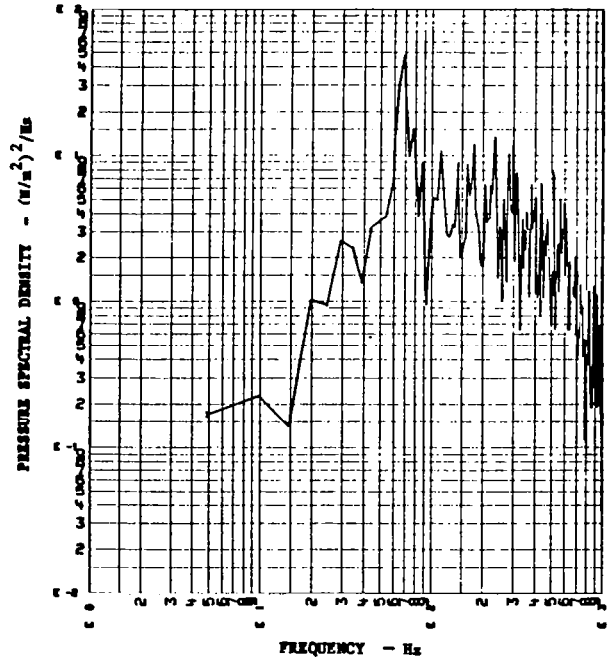

(c) Acoustic Input

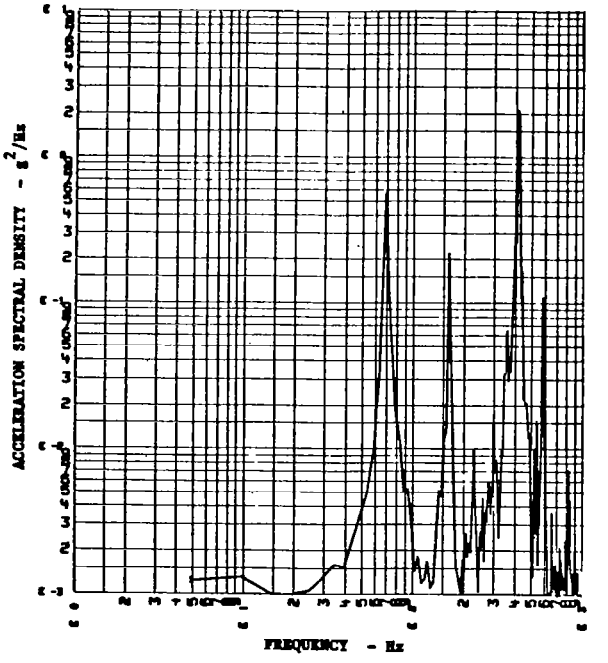

(d) Panel Response

Figure 21. - Input and response data (run 3).

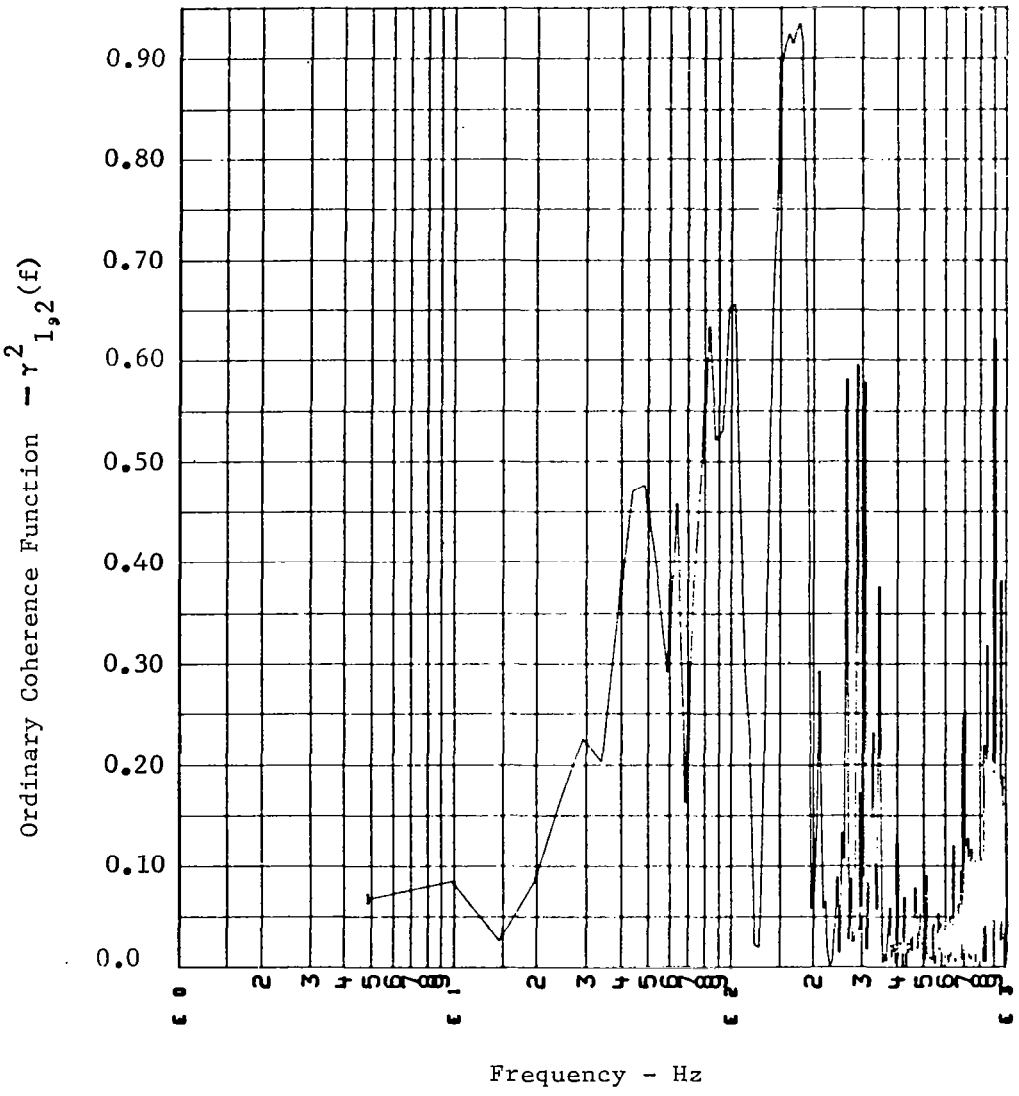

Figure 22. - Ordinary coherence function between shaker 1 and shaker 2 inputs (run 3).

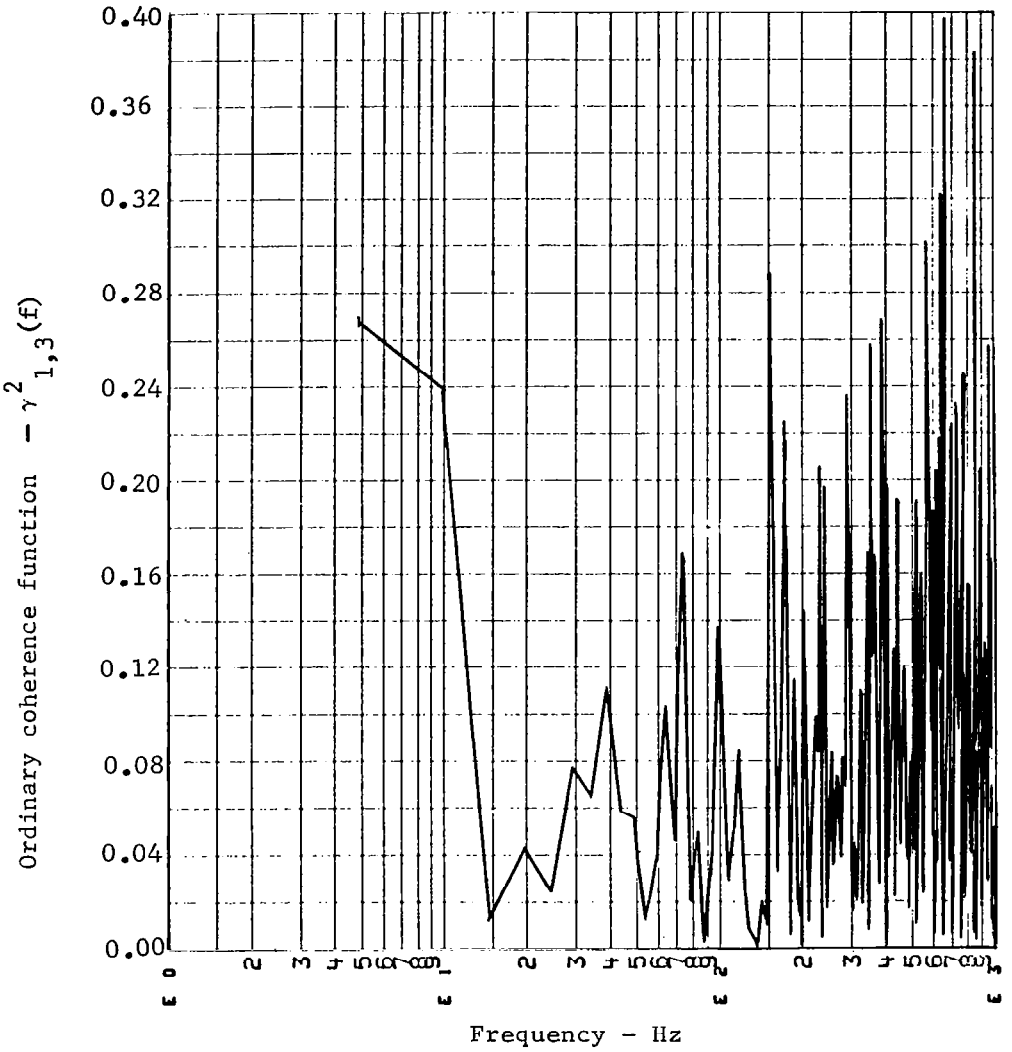

Figure 23. - Ordinary coherence function between shaker 1 and acoustics (run 3).

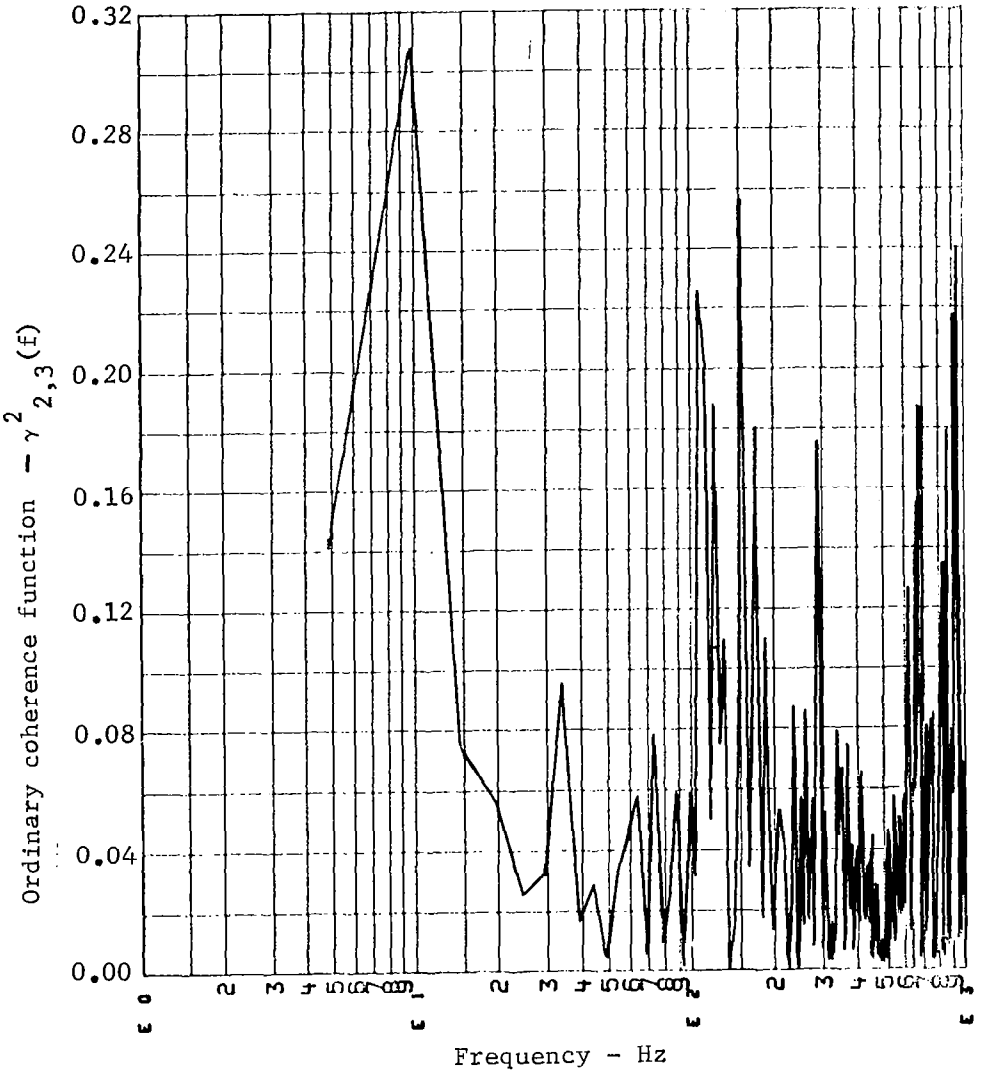

Figure 24. - Ordinary coherence function between shaker 2 and acoustics (run 3).

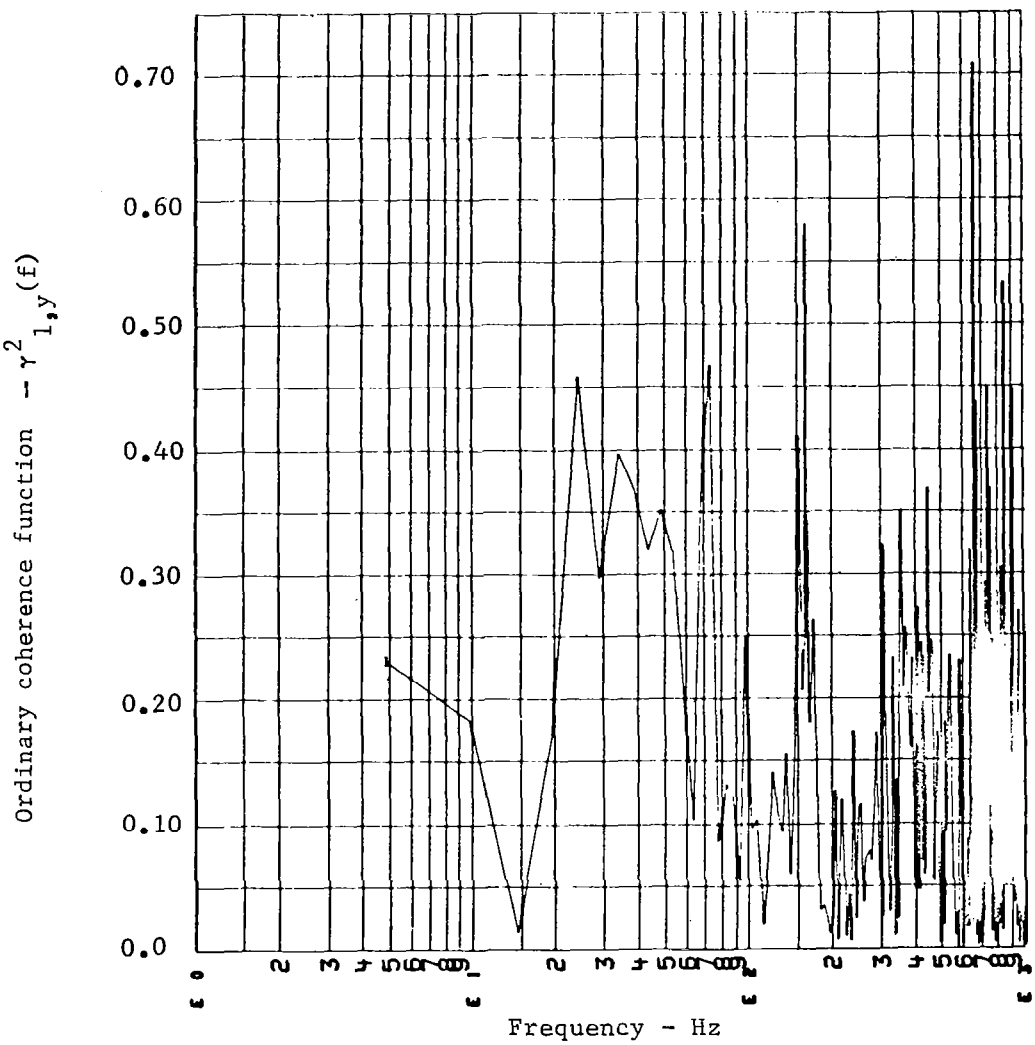

Figure 25. - Ordinary coherence function between shaker 1 input and panel response (run 3).

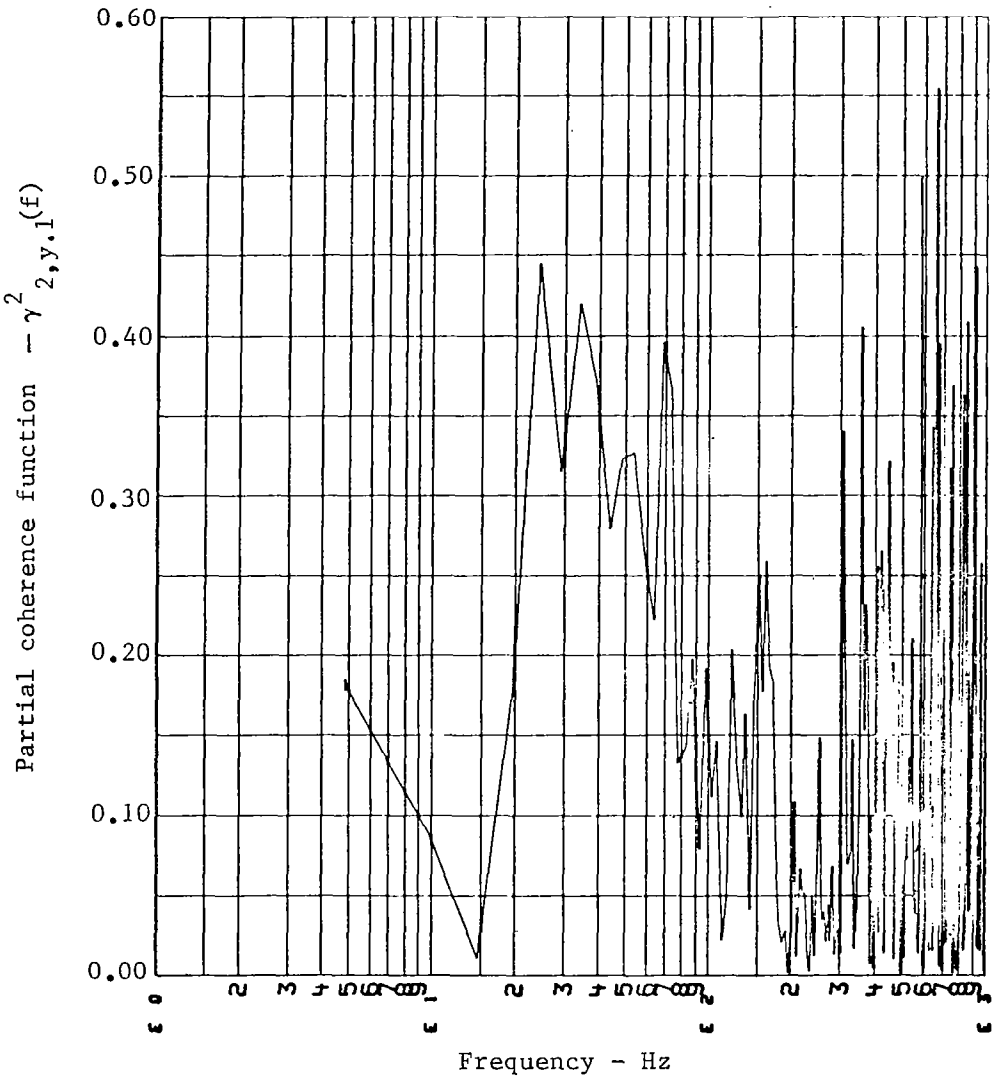

Figure 26. - Partial coherence function between shaker 2 input and panel response (run 3).

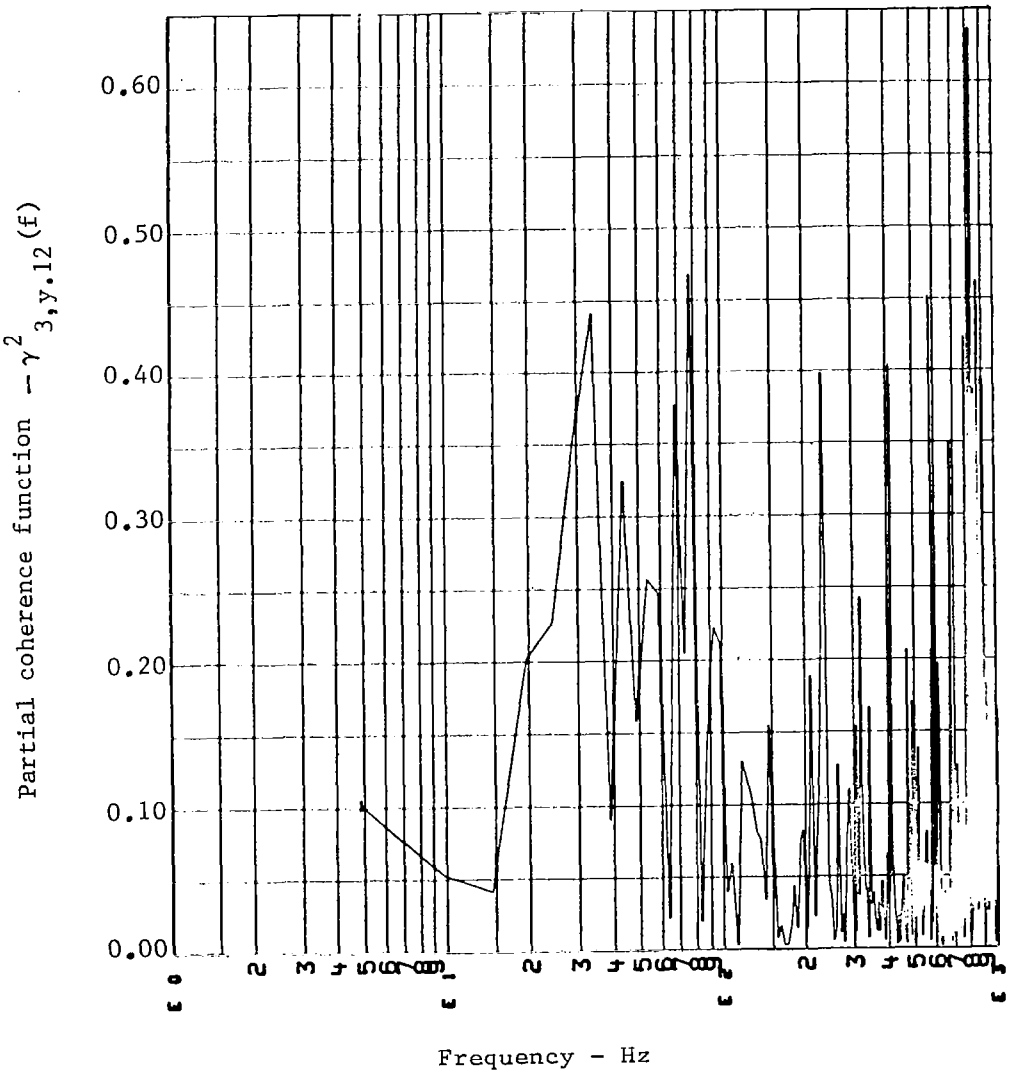

Figure 27. - Partial coherence function between acoustic input and panel response (run 3).

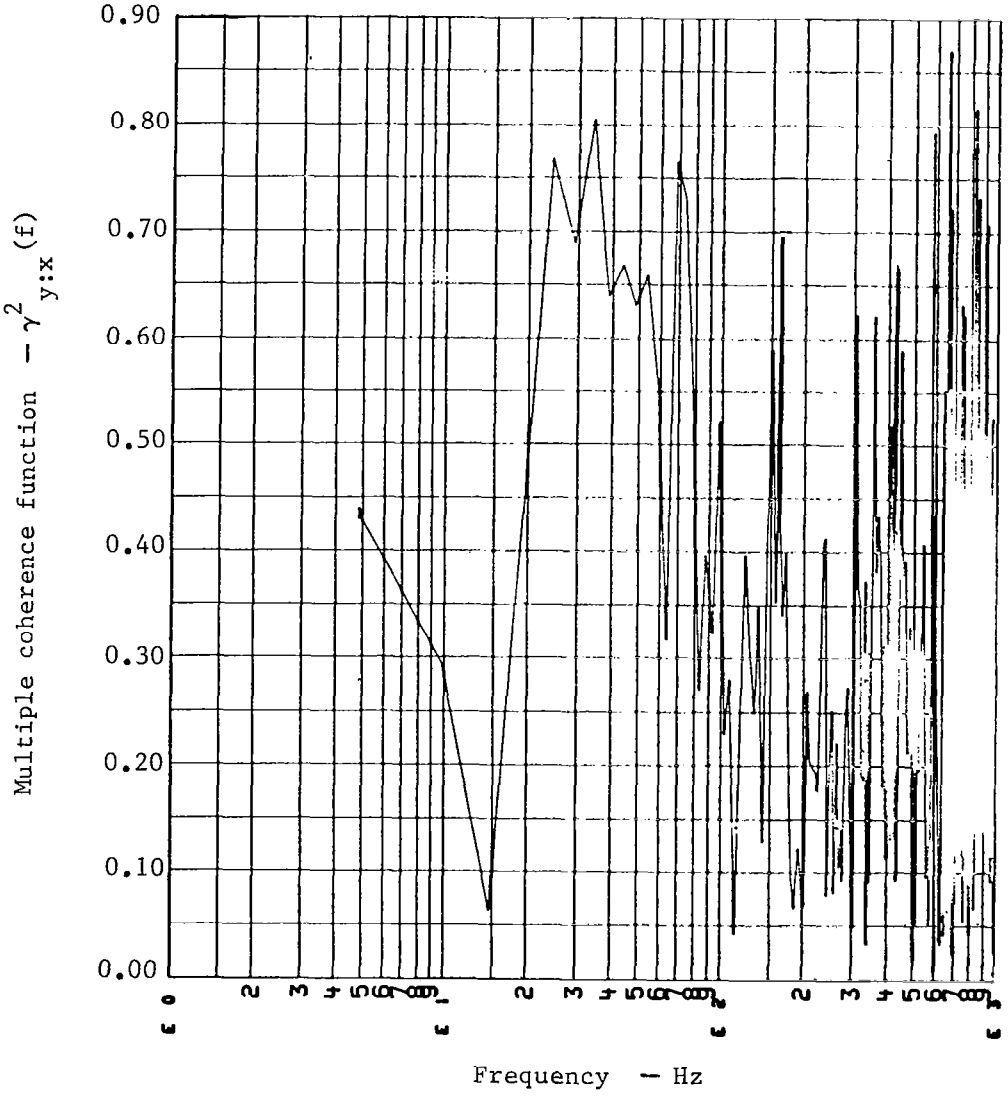

Figure 28. - Multiple coherence function between total set of inputs and panel response (run 3).

the various panel resonances, in the same way as the CFs for the run 6 data were used. Table 4 summarizes the values of the ordinary, partial and multiple coherence functions which were taken from the plots.

TABLE 4. - VALUES OF COHERENCE FUNCTIONS AT PANEL RESONANCES (RUN 3)

Frequency, Hz	γ^2_{1y}	$\gamma^2_{2y.1}$	$\gamma^2_{3y.12}$	$\Sigma\gamma^2$	$\gamma^2_{y:x}$
68	0.37	0.39	0.37	1.13	0.77
161	0.58	0.26	0.01	0.84	0.69
415	0.27	0.26	0.40	0.93	0.67
580	0.23	0.50	0.46	1.19	0.79
810	0.11	0.37	0.63	1.06	0.82

Note that the $\Sigma\gamma^2$ values are again close to unity, and in three cases actually exceed unity. This probably indicates that errors are affecting the individual CF values contributing to the summation. For example, at 68 Hz, the inputs from Shaker 1 and the acoustics are essentially independent, since γ^2_{13} is only about 0.05. Also, at 161 Hz the CF between the two shakers is greater than 0.9, so that they should probably be treated as a single input in this frequency band. The conclusion is that, to obtain the most accurate results, several different interpretations of the system would be necessary, changing the model as appropriate for different frequency ranges as indicates by the mutual coherence between the inputs.

Run 4 (shaker 1 only). - The objective of this run was to supplement the data from Runs 2 and 3 and to identify the amount of "noise" in the system. The OCF for the single input/single output system would be 1.0 across the full frequency range in the absence of noise or nonlinearities. Figure 29 shows the input and response data. The plots are very similar to those obtained from Run 4 which, as discussed earlier, was effective as a single input/single output case. The response data plot shows high peaks at 68 and 161 Hz. These were the frequencies at which the shakers were responsible for most of the response, according to the interpretation of the associated PCFs. Thus, the Run 4 data support that interpretation. Figure 30 is a plot of the OCF and is similar to the OCF plots (Figures 10 and 11) from Run 1. These show that the analyzed data have a high noise level at most frequencies in the range 5 to 1000 Hz. Low damping and, hence, low off-resonance response and narrow frequency bands contribute to this problem.

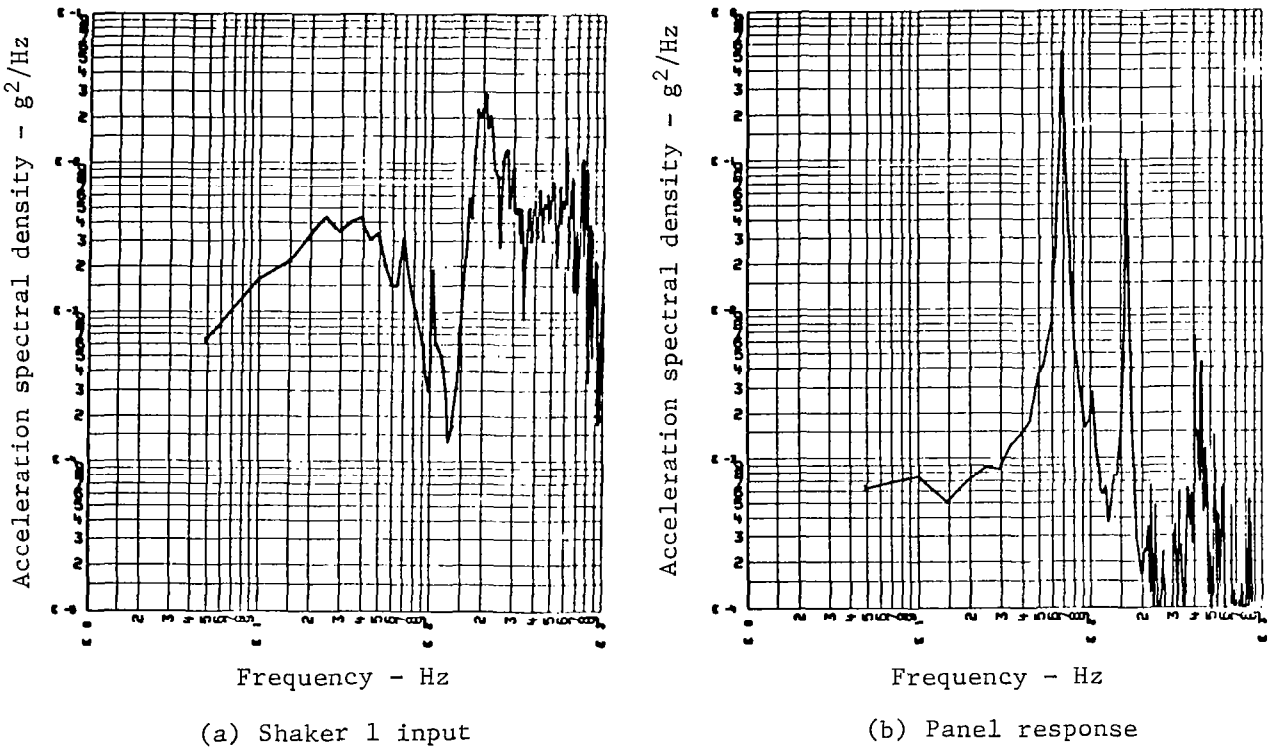

(a) Shaker 1 input

(b) Panel response

Figure 29. - Input and response data for run 4 .

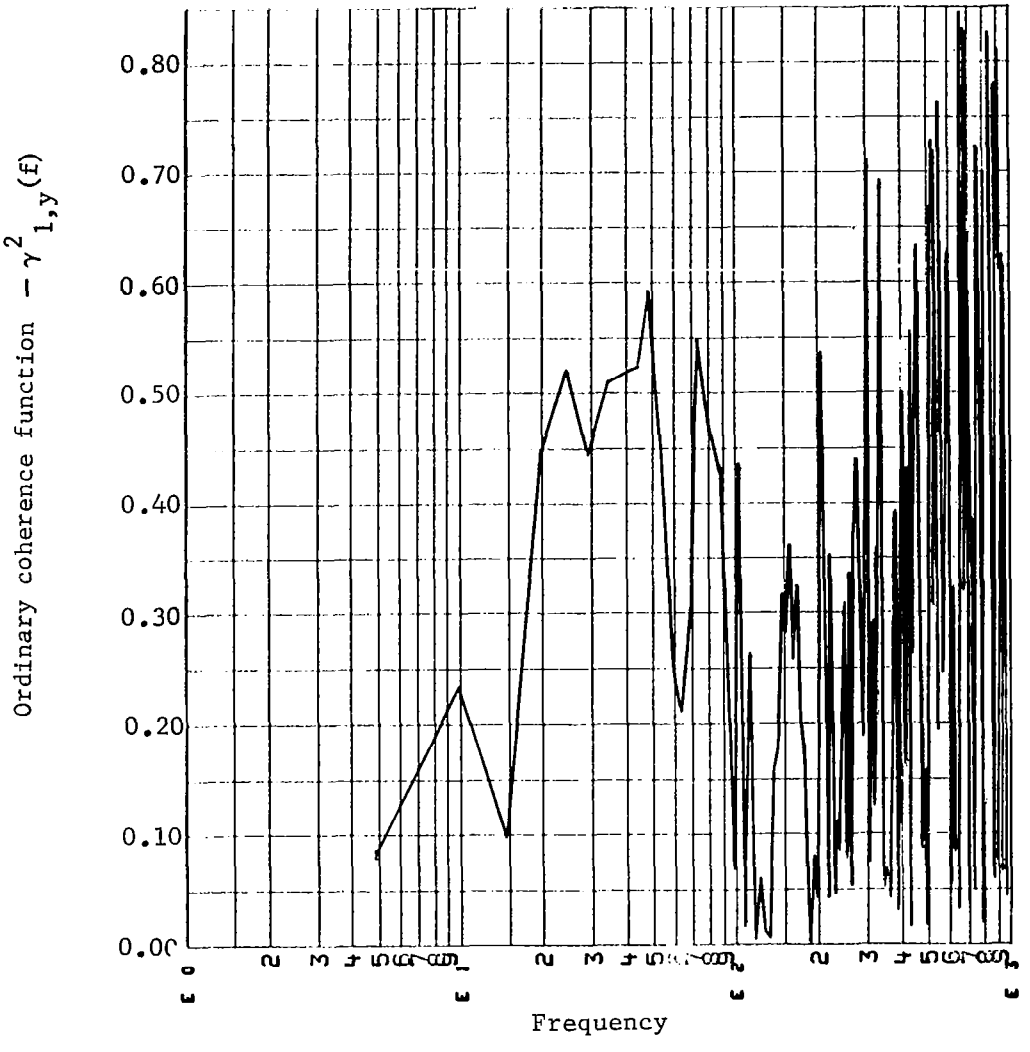

Figure 30. - Ordinary coherence function between shaker 1 input and panel response (run 4).

The Run 4 data were also used to investigate the effect of varying the number of data segments used in the averaging process before calculating the OCF. Figure 31 shows four versions of the OCF, in which 10, 50, 100, and 200 averages were used. With only four different cases, the results were not conclusive; however, as illustrated in Table 5, the variation of some frequencies was large enough to suggest that a number of averages in the region of 200 is necessary to ensure reasonable accuracy. On the other hand, if a fixed record length of data is available for analysis, the accuracy of the results will be degraded if the length of each segment is reduced, so a detailed error analysis is necessary to ensure that the best trade-off is made.

TABLE 5. - EFFECT OF AVERAGING ON OCF VALUES

Frequency, Hz	No. of averages	Value of OCF
44	10	0.69
	50	0.52
	100	0.52
	200	0.55
110	10	0.41
	50	0.43
	100	0.48
	200	0.58
400	10	0.60
	50	0.50
	100	0.46
	200	0.40
660	10	0.91
	50	0.85
	100	0.77
	200	0.74

Finally, data from Run 4 were used to plot the OCF in a slightly different format, using linear scales for both coherence function and frequency. The result is shown in Figure 32 and is based on using 200 averages. The frequency resolution is worse at low frequencies and better at high frequencies than the comparable semilog plot, and the preferred format will depend on the particular application.

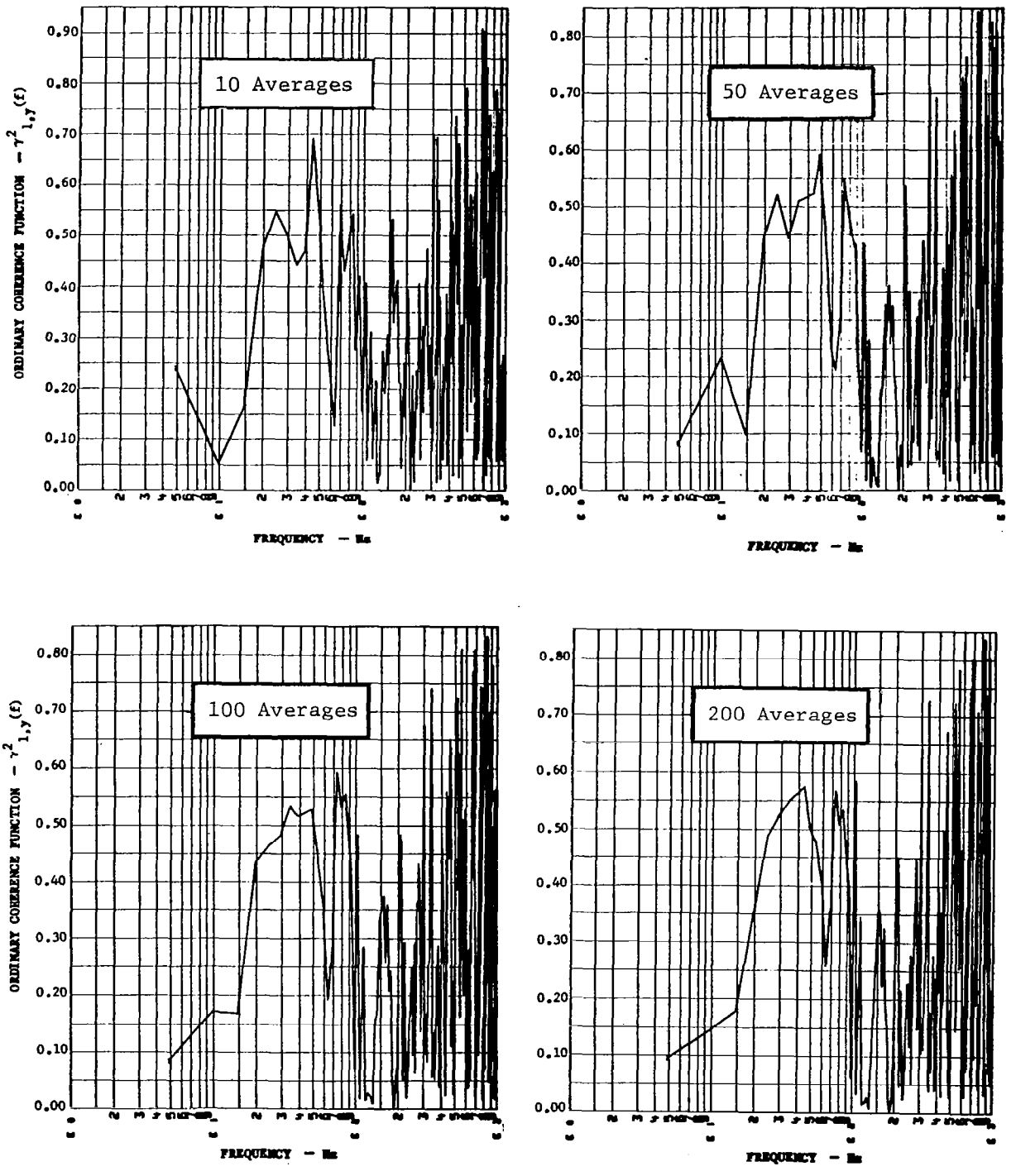

Figure 31. - The effect of number of samples on the estimate of ordinary coherence function (run 4).

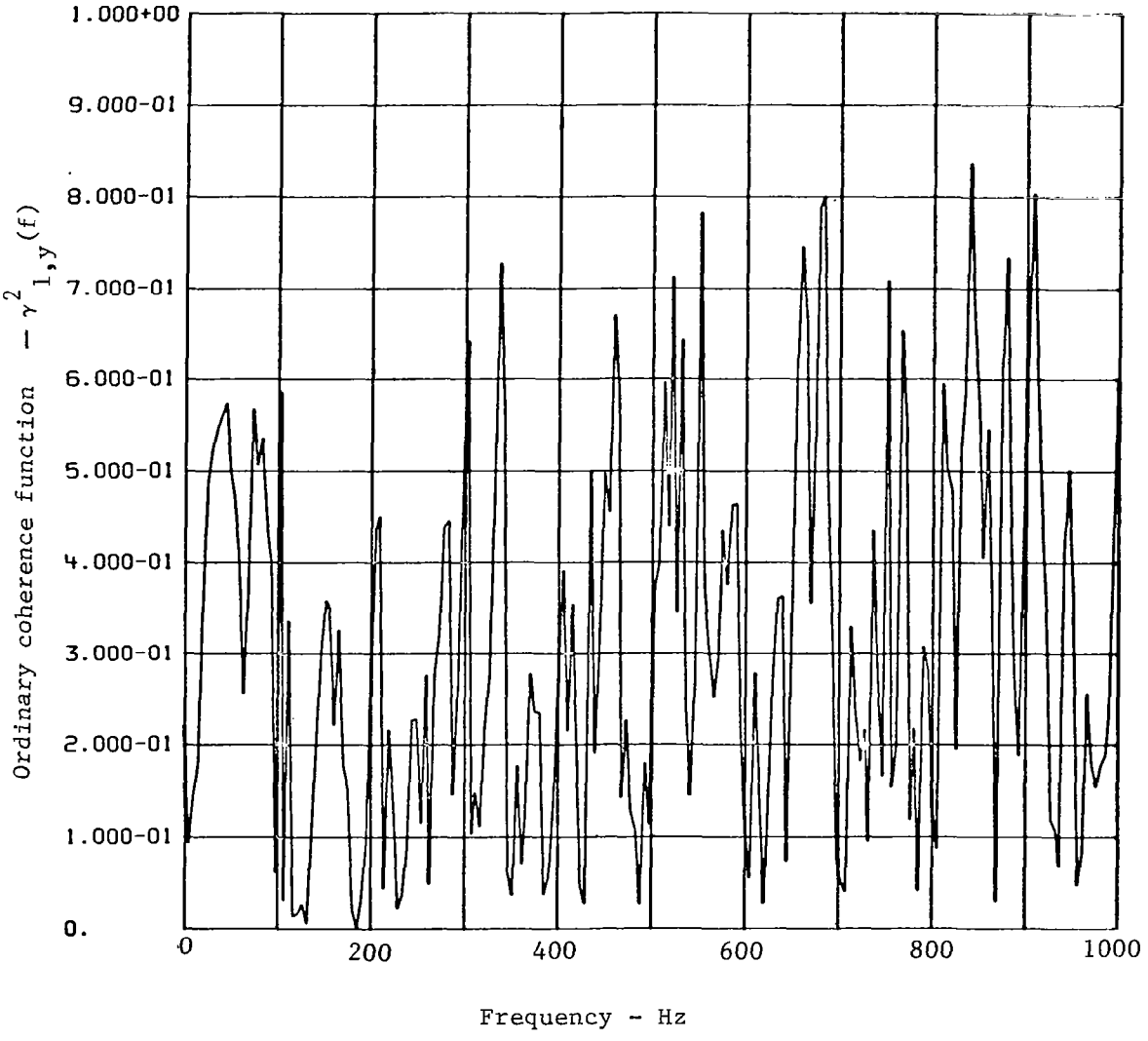

Figure 32. - Ordinary coherence function between shaker 1 input and panel response, using 200 averages, with linear frequency scale (run 4).

Run 5 (acoustics only). - This run, like Run 4, was intended to supplement Runs 2 and 3. Since the panel response in this run was caused only by acoustics, it can be compared with the acoustically-induced responses in Runs 2 and 3, as indicated by the PCFs ($\gamma^2_{3y.12}$). In the discussion of the Run 2 results, it was concluded that the responses at 290 and 420 Hz were caused primarily by the acoustics. The response plot in Figure 33(b) supports this conclusion strongly at 420 Hz, and to a lesser extent at 290 Hz. The OCF plot in Figure 34 again shows that significant noise and/or nonlinearity effects contaminated the measured data.

Run 6 (shaker 1 plus acoustics). - Two nominally uncorrelated inputs were used for this test run. Figure 35 shows the input and response data. As usual, the coherence between the inputs was first calculated to verify that the assumption of independence was correct. Figure 36 shows that this was the case except at the 4.8 Hz point and at some frequencies above 500 Hz when the value of the OCF exceeded the Bendat criterion of 0.10 by a small margin. It was concluded that it would be reasonable to ignore this degree of mutual coherence and treat the system inputs as uncorrelated.

The OCF plots between each input and the output appear in Figures 37 and 38. When these are reviewed in conjunction with panel response plot in Figure 35(c), it is clear that the response peaks at 68 and 160 Hz are due primarily to the shaker input, while the resonance at 420 Hz appears to be driven most efficiently by the acoustics. The MCF plot in Figure 39 again shows that a high degree of "noise" is present in the data.

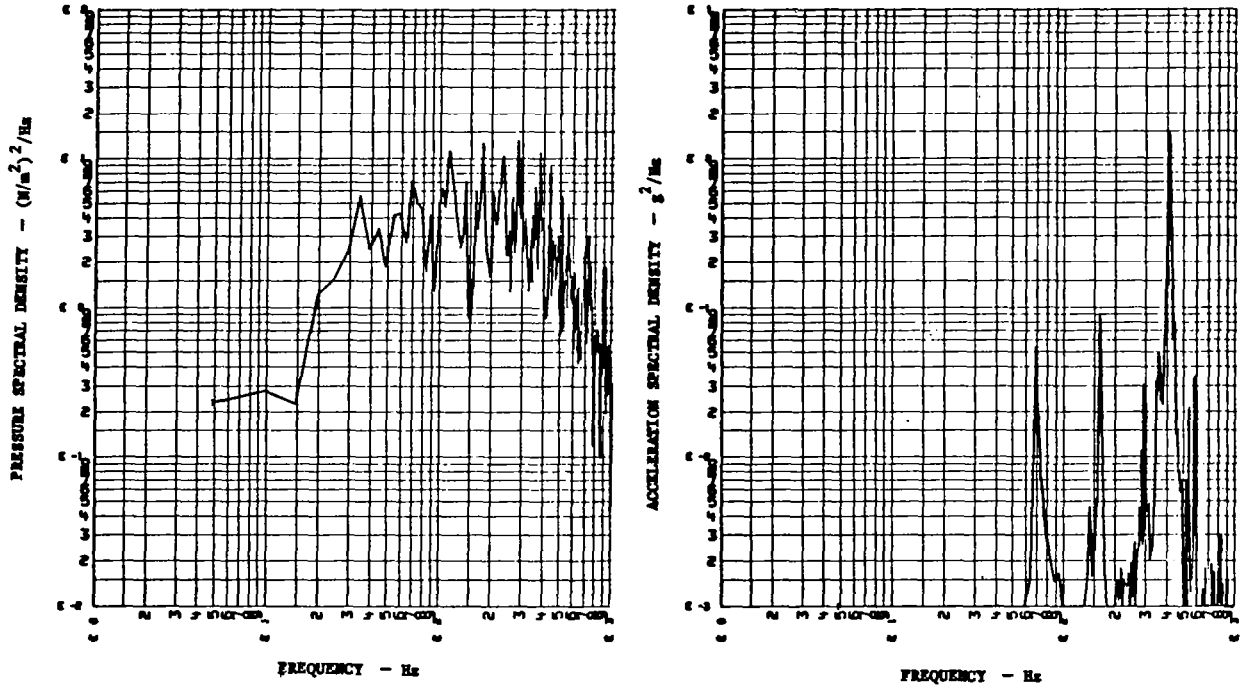

(a) Acoustic input

(b) Panel response

Figure 33. - Input and response data (run 5).

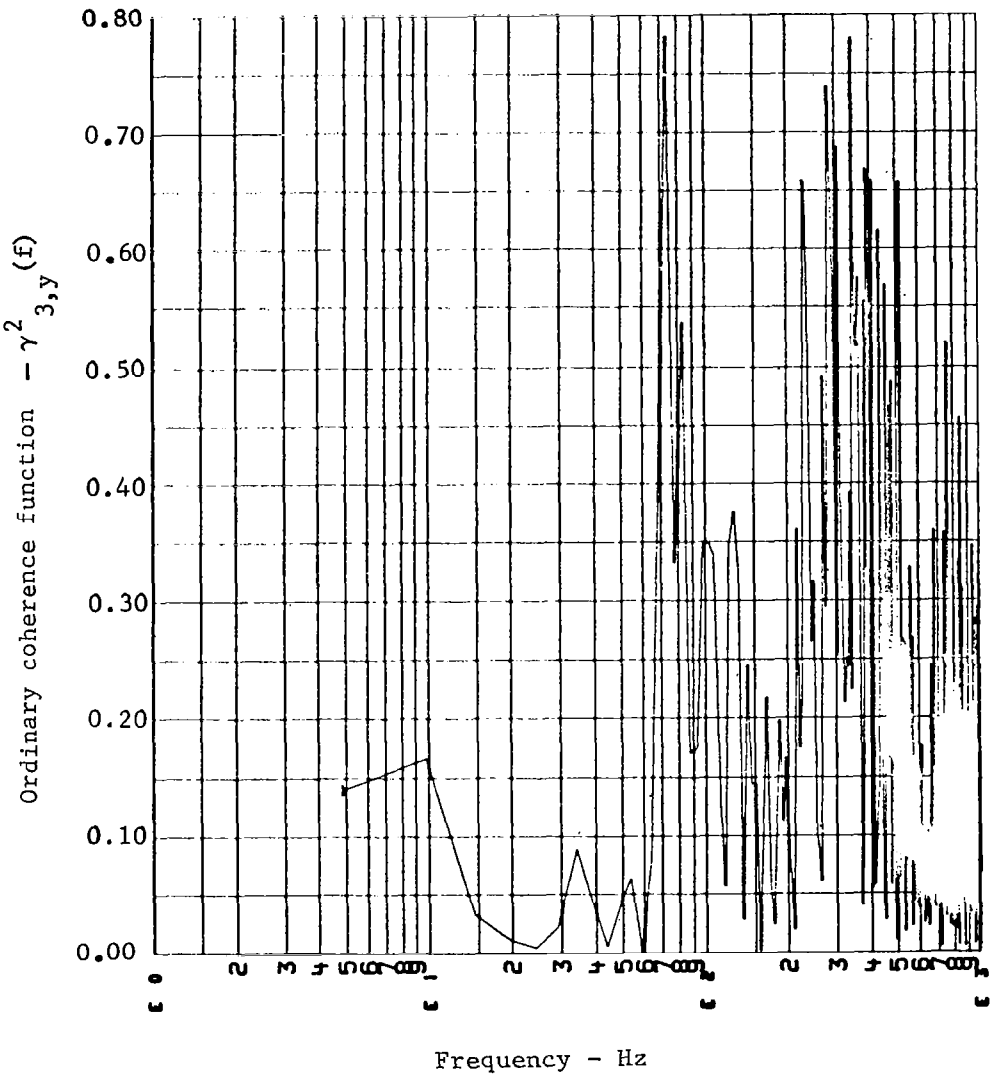

Figure 34. - Ordinary coherence function between acoustic input and panel response (run 5).

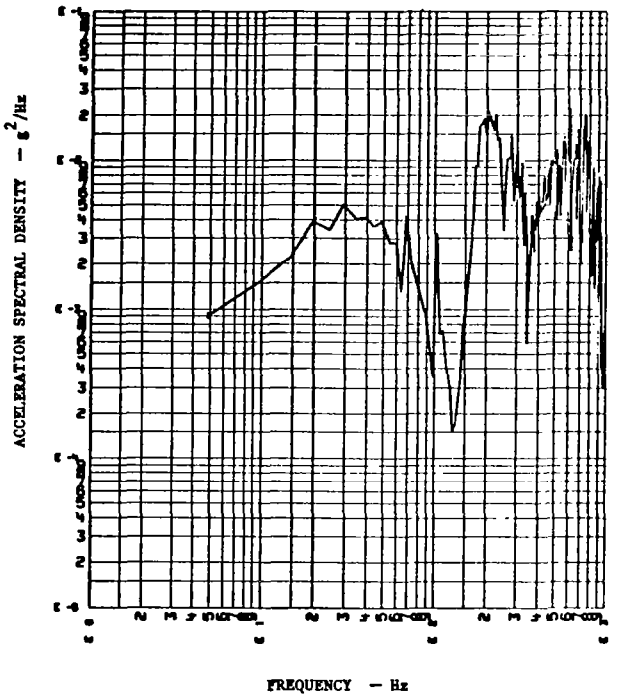

(a) Shaker 1 input

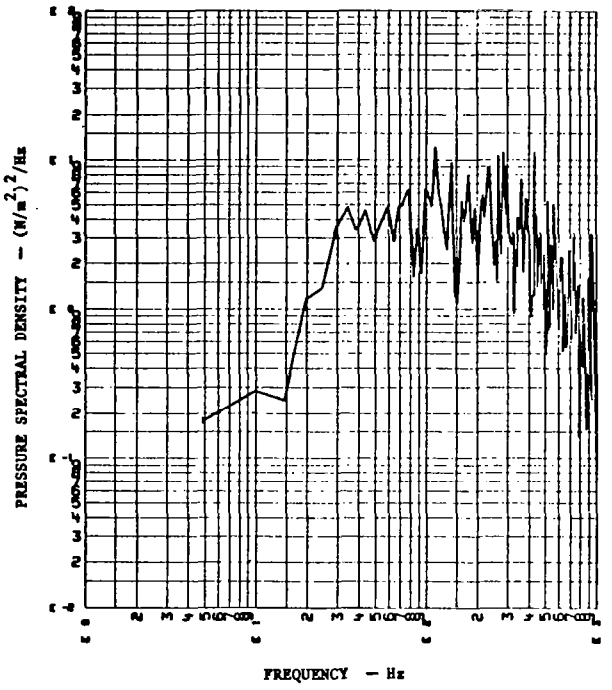

(b) Acoustic input

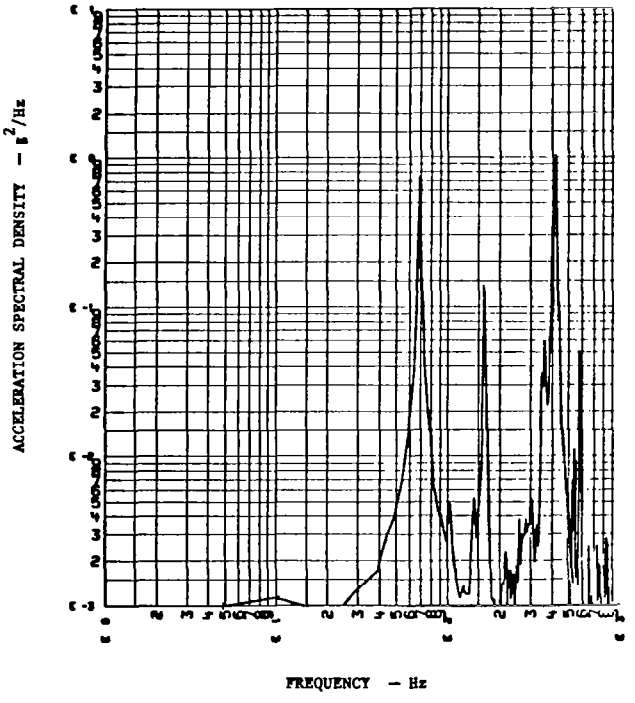

(c) Panel response

Figure 35. - Input and response data (run 6).

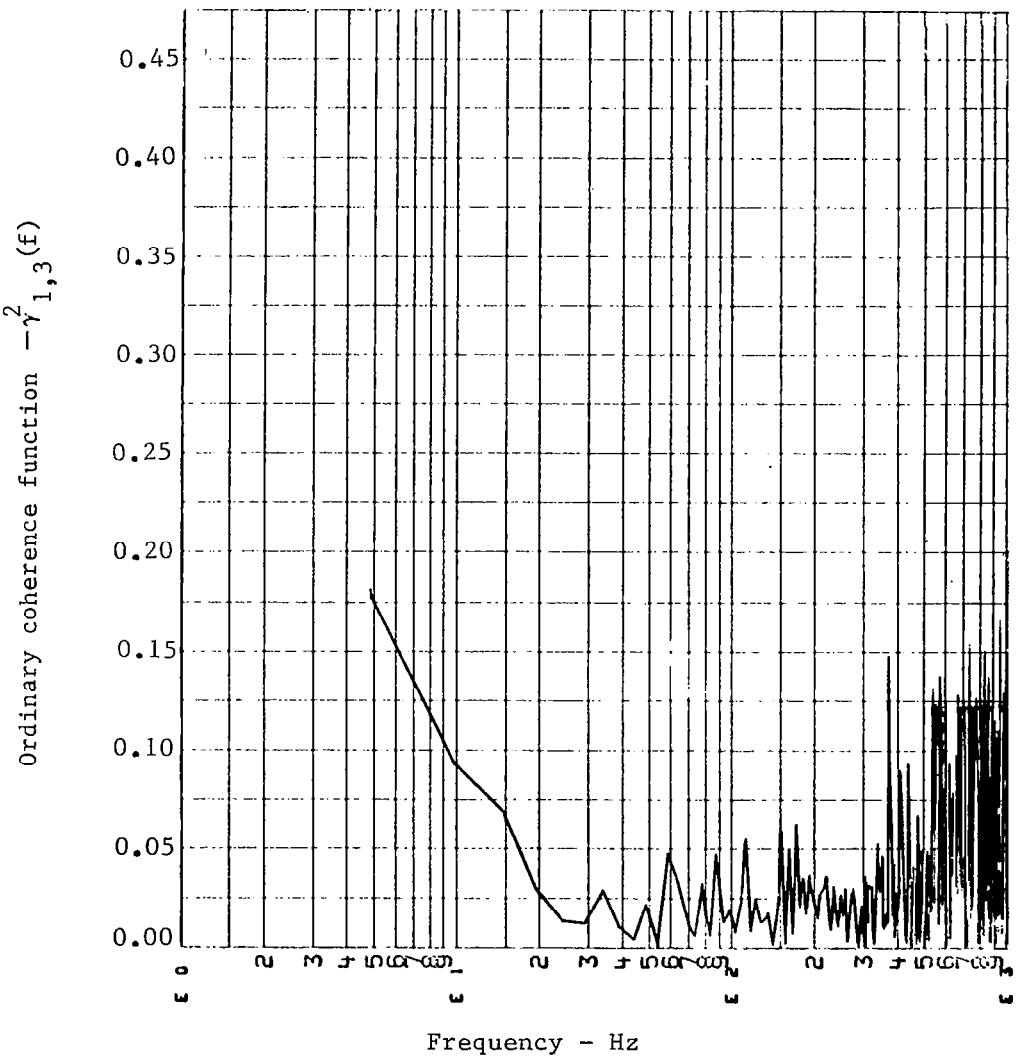

Figure 36. - Ordinary coherence function between shaker 1 input and acoustics (run 6).

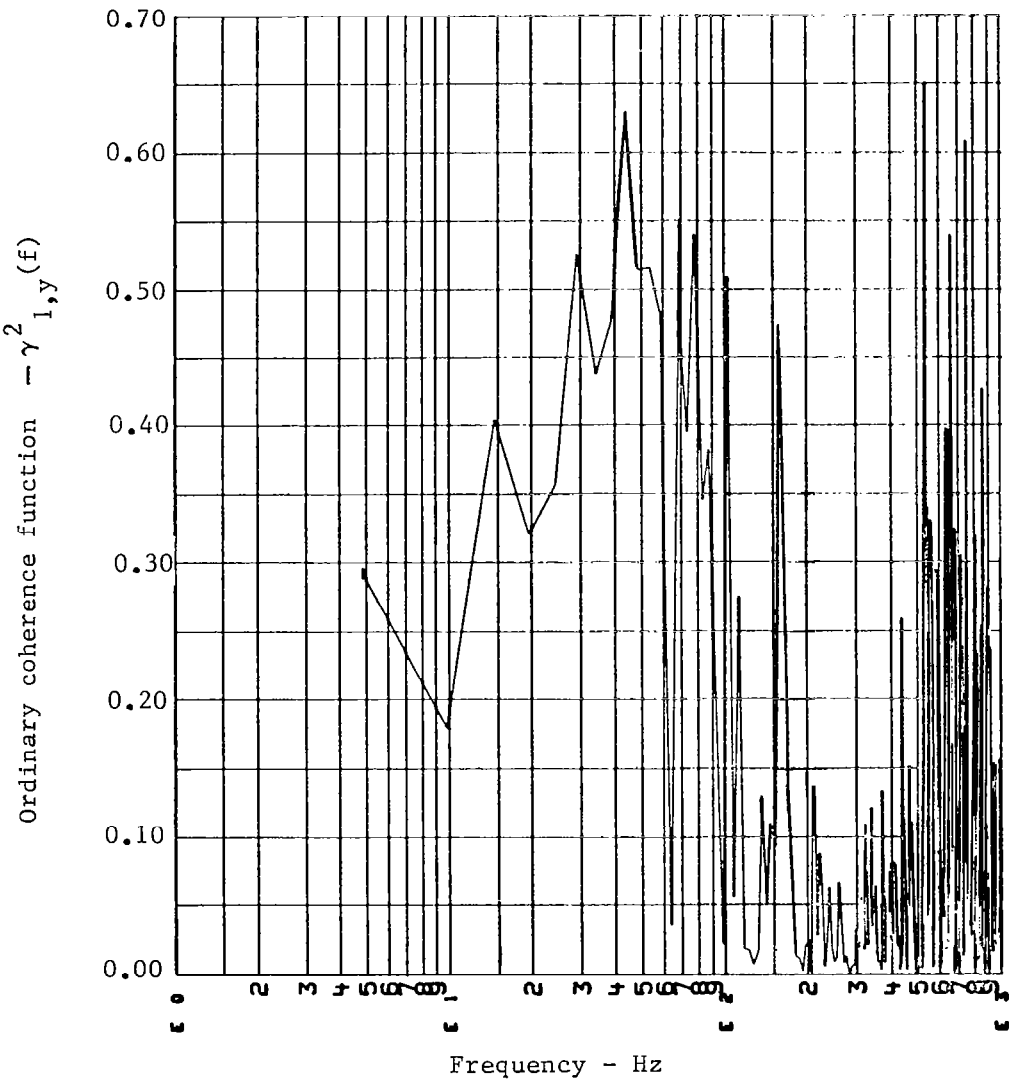

Figure 37. - Ordinary coherence function between shaker 1 input and panel response (run 6).

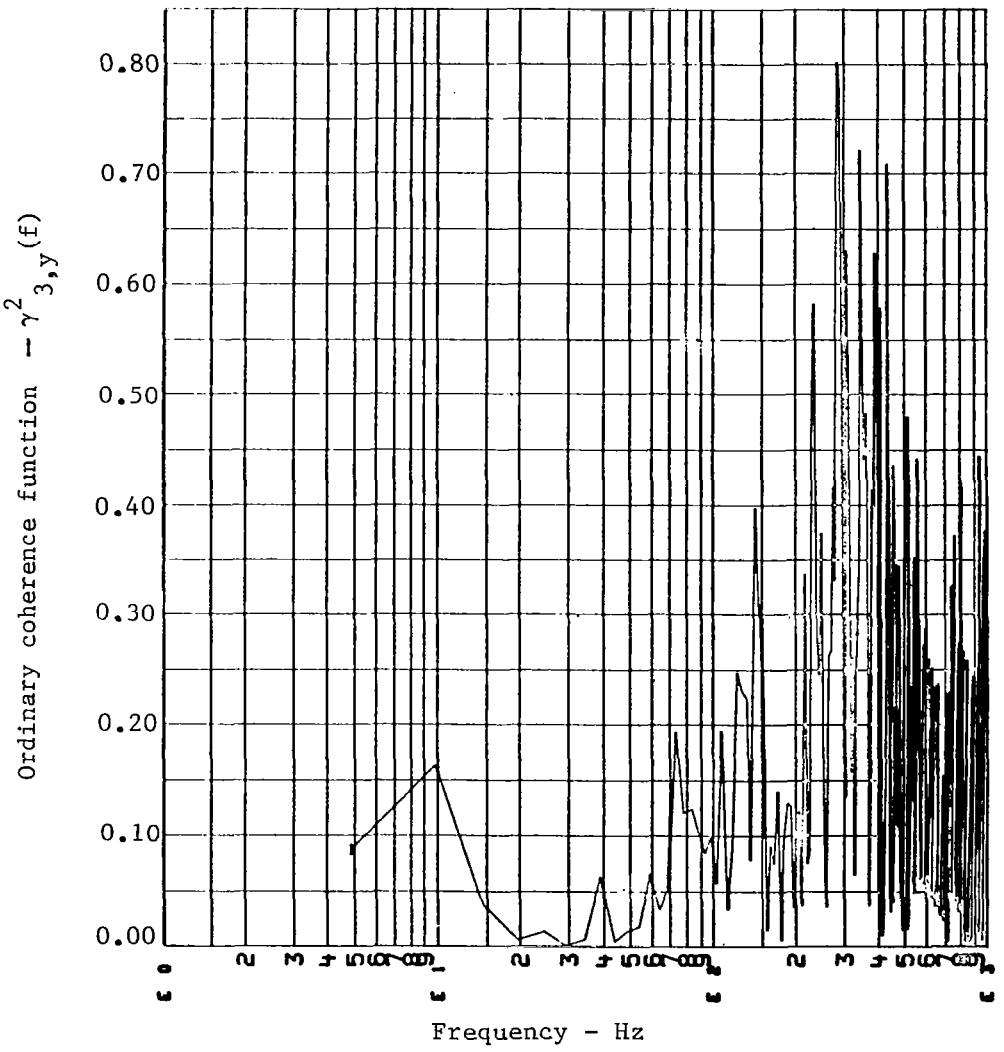

Figure 38. - Ordinary coherence function between acoustic input and panel response (run 6).

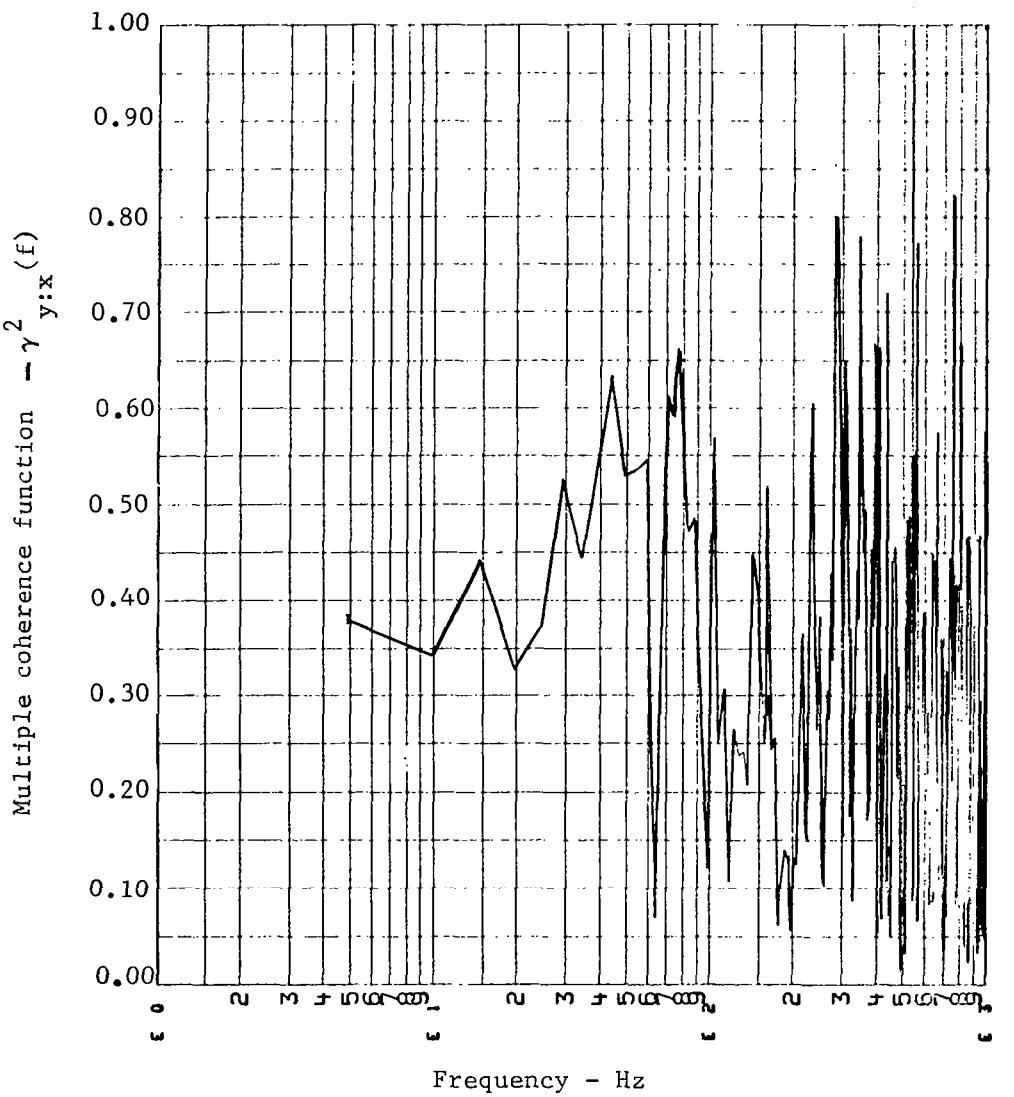

Figure 39. - Multiple coherence function between total set of inputs and panel response (run 6).

Phase II: Nonstationary Inputs

Data from Run 7 were used to investigate the application of the CF approach to a system with two obviously nonstationary uncorrelated inputs. The inputs were a single shaker plus acoustics, and were initially identical to those used in Run 11 (see Fig. 35). After applying the stationary inputs for a few seconds, the overall acceleration and sound pressure levels were gradually increased to peak values approximately 8 dB above the initial values, and then reduced back to the initial values. The time variation of the overall levels was as shown below:

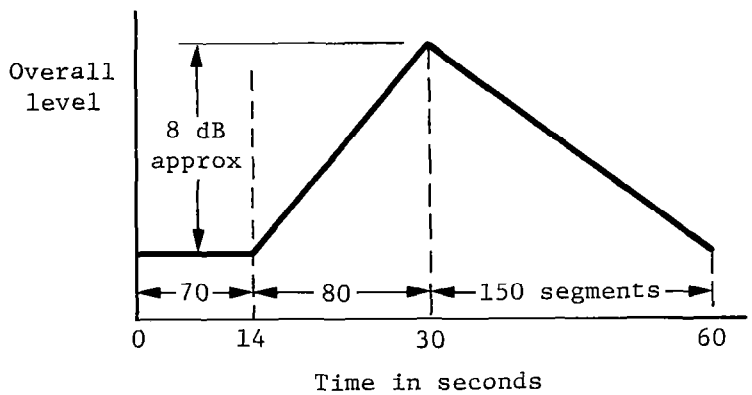

To obtain a basis for comparison, the OCFs between the individual inputs and the response were calculated using data from the first 14 seconds, when the inputs were stationary.

The roll-off part of the time history consisted of the last 30 seconds of the test, equivalent to 150 data segments after digitizing. This was used for the nonstationary analysis. Six different data records, each containing 20 data segments, were extracted by the following method:

(1) For the first data record, the first 20 segments out of the 140 available were used to calculate two OCFs.

(2) For the second record, alternate segments out of the first 40 were employed for the calculation.

(3) The third record was made up by taking every third segment until 20 segments were accumulated.

(4) For record #4, every fourth segment from the first 80 segments was used.

(5) The fifth and sixth records were made up in the same way, utilizing every fifth and sixth segment respectively.

The six different analyses thus covered a range in record lengths of approximately 4 to 24 seconds, with a corresponding spread of about 6 dB (factor of 2) on the overall levels of the inputs.

Figure 40 shows the OCF between the shaker input and the panel response for the stationary precursor in Run 7. Figures 41 and 42 give the same OCF for the six increasingly nonstationary time records. The OCF between the acoustic input and the panel response for the stationary case and the six nonstationary cases is plotted in Figures 43, 44, and 45.

A comparison of $\gamma^2_{1,y}$ for the stationary part of the run, plotted in Figure 40, with the same OCF computed from the six nonstationary time records (Figures 41 and 42) shows that the general shape of the OCF is similar for all seven conditions. However, large variations occur in the magnitude of the OCF, with no apparent relationship to the length of the time record. An inspection of the plots for $\gamma^2_{3,y}$ leads to the same conclusion; that the introduction of nonstationarity to the inputs causes the OCF to change significantly, but not in a predictable way.

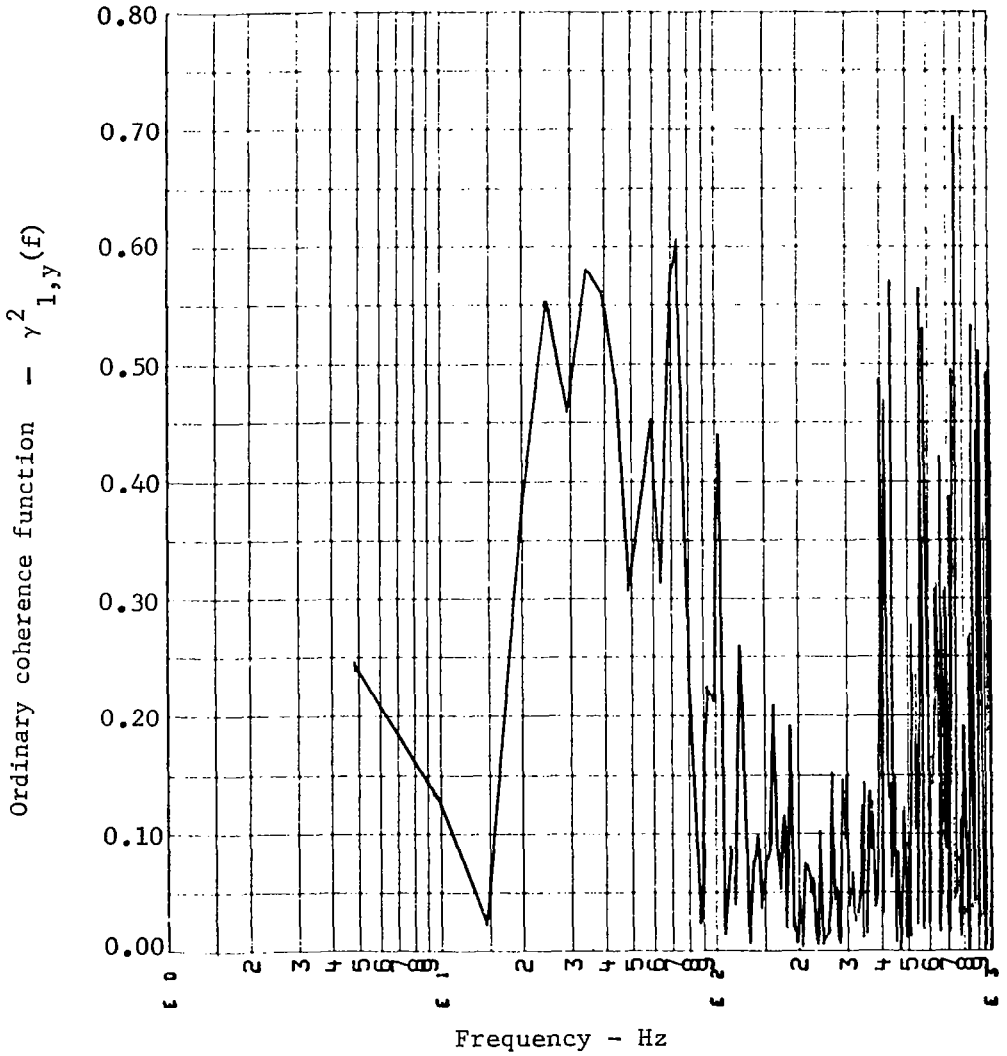

Figure 40. - Ordinary coherence function between shaker 1 input and panel response, stationary part of (run 7).

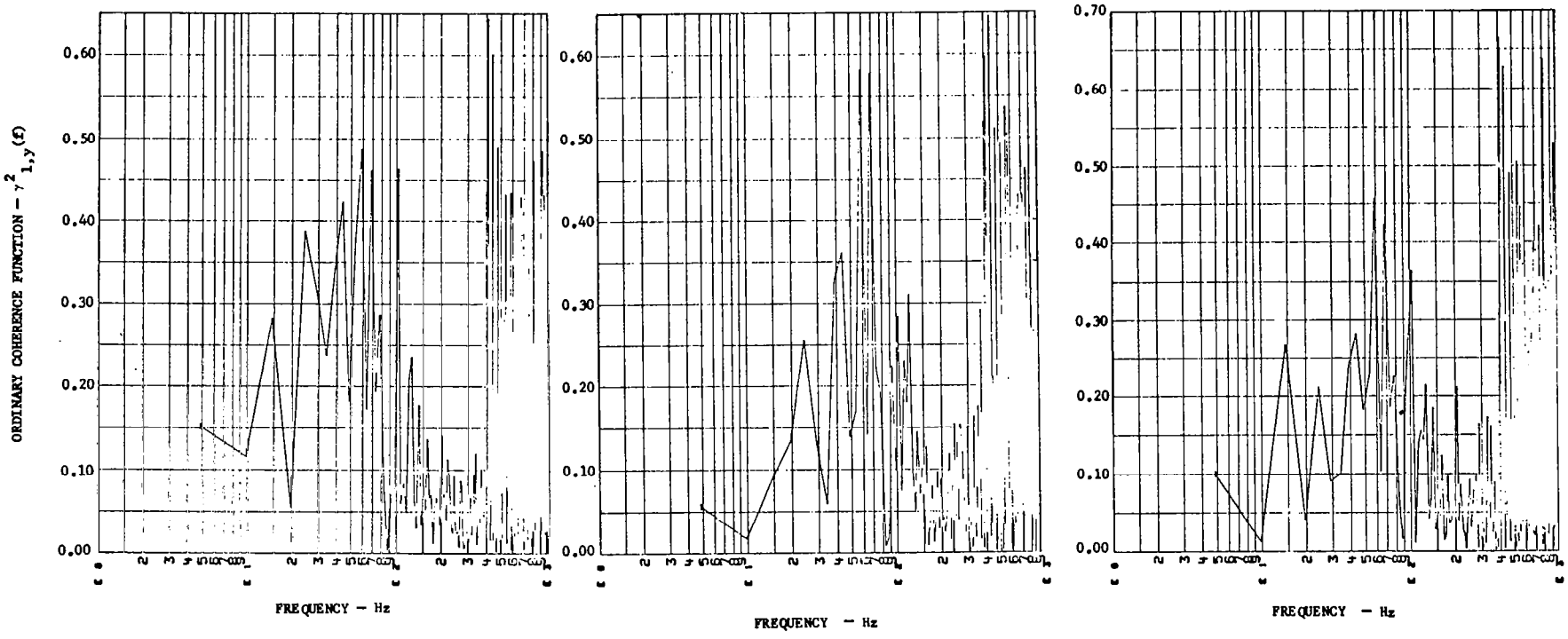

(a) Data record 1 (b) Data record 2 (c) Data record 3

Figure 41. - Ordinary coherence function between shaker 1 input and panel response, nonstationary part of run 7 .

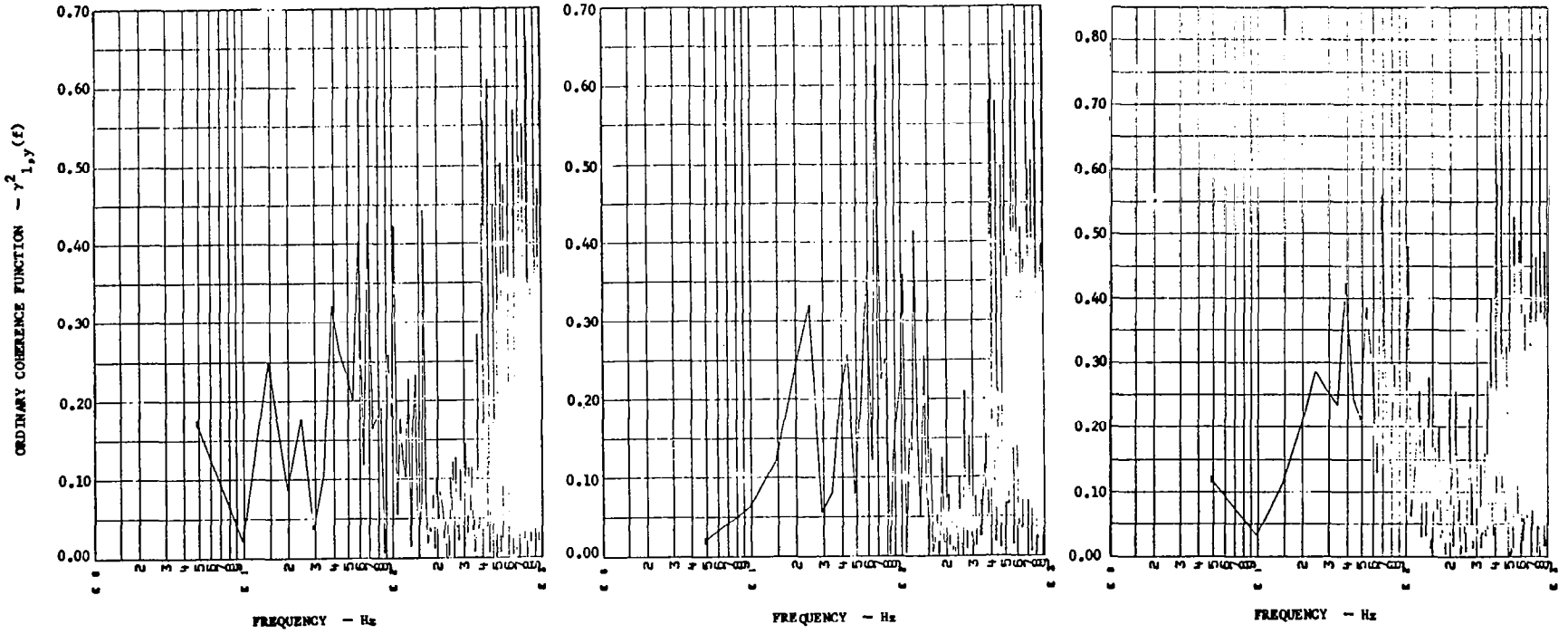

(d) Data record 4 (e) Data record 5 (f) Data record 6

Figure 42. - Ordinary coherence function between shaker 1 input and panel response, nonstationary part of run 7 .

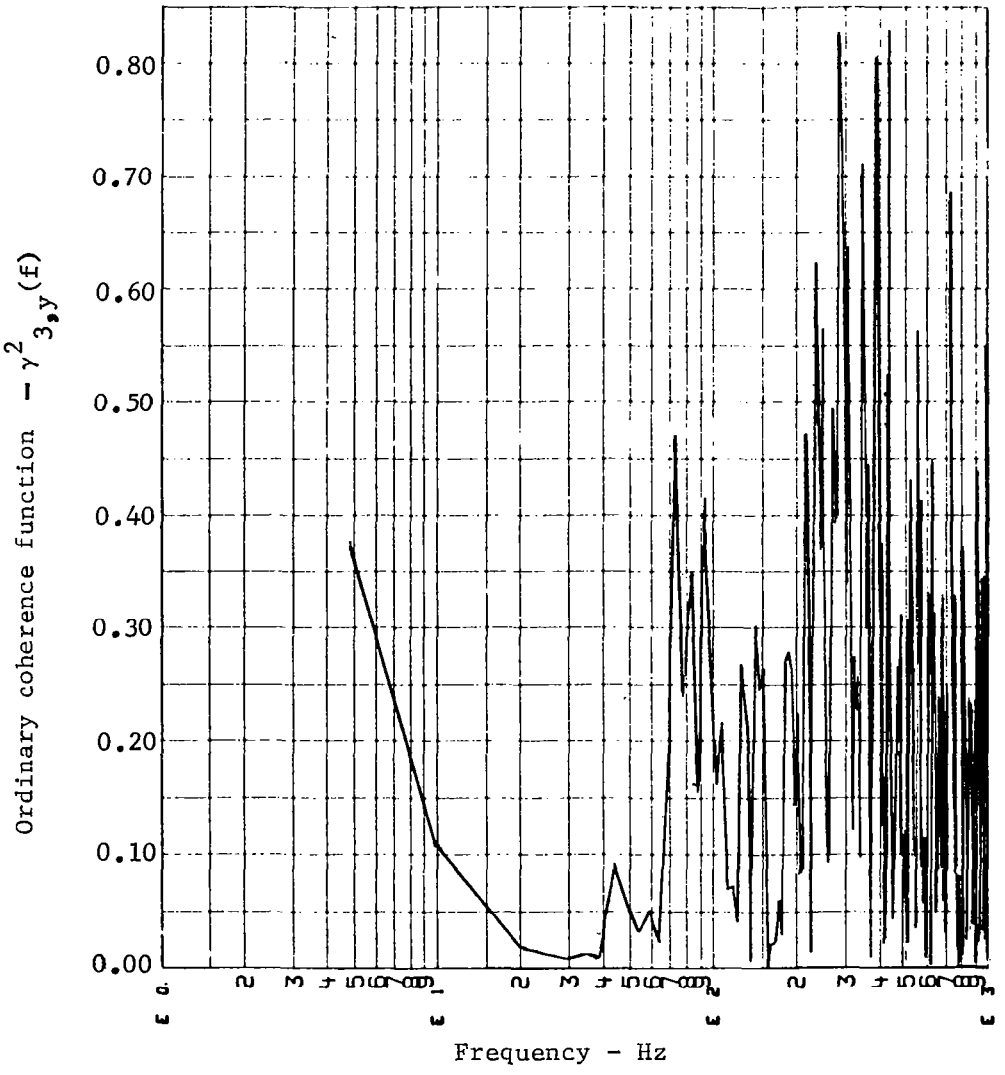

Figure 43. - Ordinary coherence function between acoustic input and panel response, stationary part of run 7 .

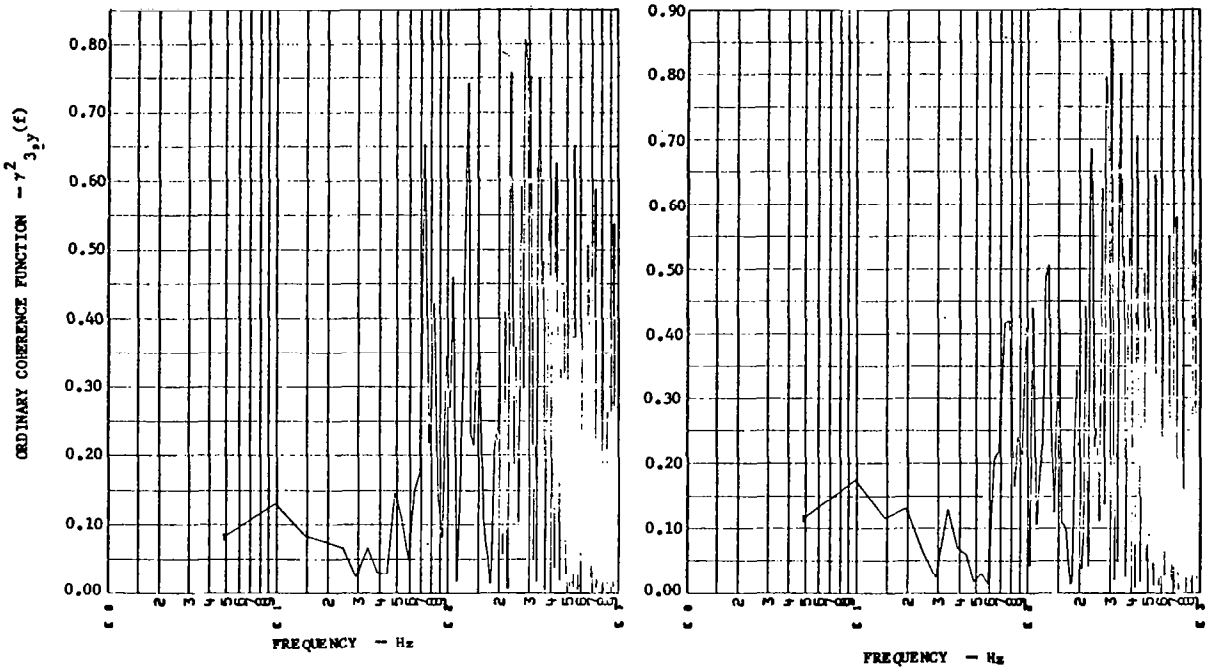

(a) Data record 1

(b) Data record 2

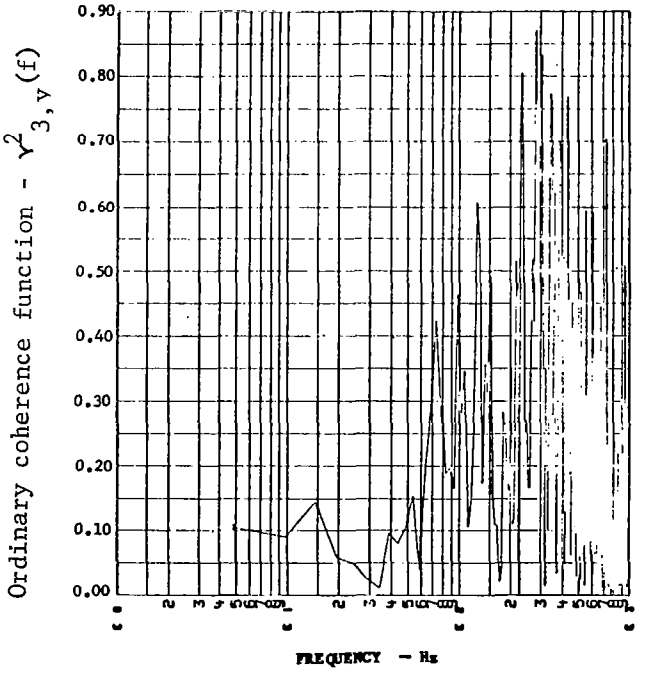

(c) Data record 3

Figure 44. - Ordinary coherence function between acoustic input and panel response, nonstationary part of run 7 .

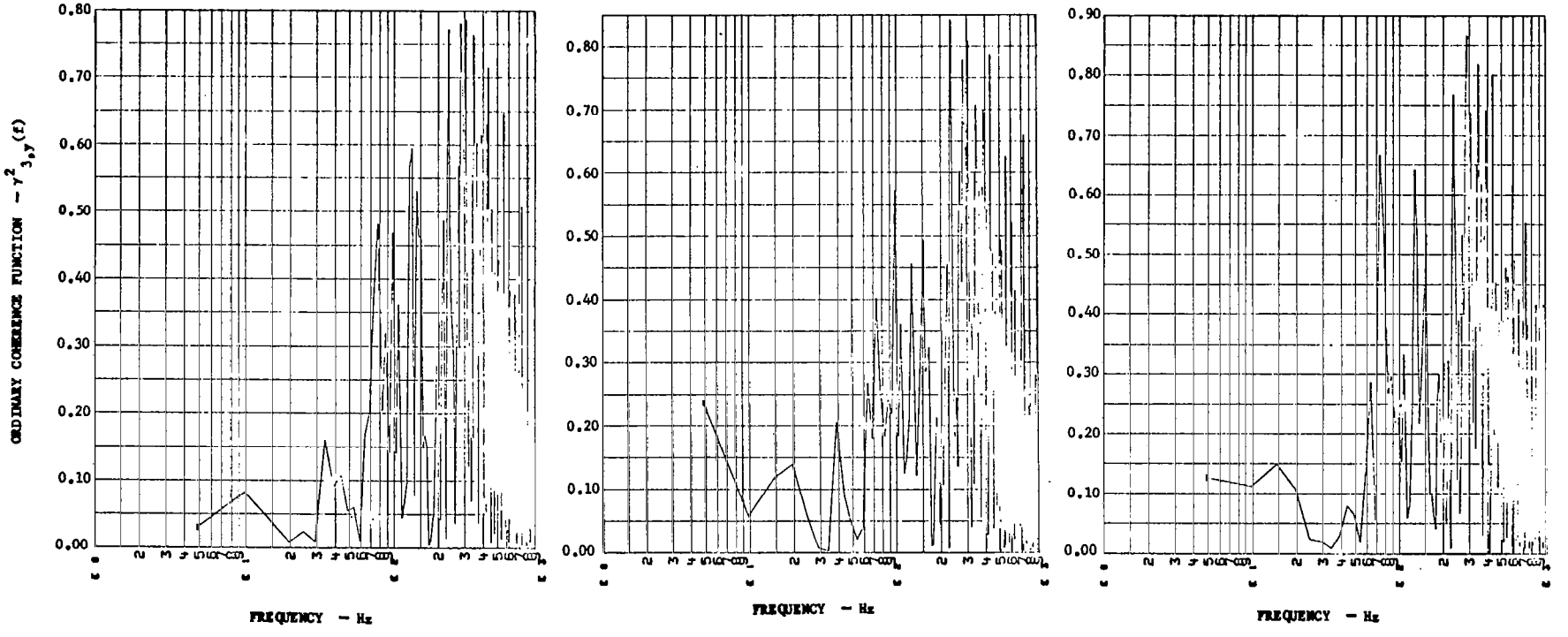

(d) Data record 4

(e) Data record 5

(f) Data record 6

Figure 45. - Ordinary coherence function between acoustic input and panel response, nonstationary part of run 7 .

CONCLUSIONS

Phase I: Stationary Inputs

From the results of Phase I of the study, it was concluded that the coherence function technique is effective in identifying the relative contributions of multiple sources of dynamic excitation to the response of a practical mechanical system. However, this was found to be true, for the system tested, only in the region of resonant response frequencies. The technique did not give good results at frequencies between resonances, when errors induced by noise and/or system nonlinearities were apparently similar in magnitude to the quantities being used in the calculation. This is not a serious handicap when using the technique strictly for source identification, since such information is generally of greatest interest at resonant frequencies, but may seriously hinder applications in which general inputs are being deduced from the response of a specific resonant system. The noise levels were high in all of the test cases, as indicated by the fact that the multiple coherence function approached unity only at a relatively few frequency points. For an ideally linear and noise-free system, the MCF should have a value of 1.0 across the full frequency band if all the appropriate inputs have been properly included.

The iterative approach developed by Bendat (Refs. 3 and 7) was used to calculate the partial coherence functions for the cases involving correlated inputs. A comparison of this approach with the older matrix-based formulation (Refs. 4, 5, and 6) showed the iterative method to be conceptually simpler, and probably more economical in computer time, especially as the number of correlated inputs increases. To verify this conclusion, it would be necessary to analyze an appropriate model by both methods then make a direct cost comparison.

To find out whether the inputs to the system were correlated or not, it was necessary to calculate the OCF between the various inputs; if the value of the OCF was no greater than 0.1, then it was assumed that the two inputs involved were uncorrelated so that the source identification could be carried out in terms of OCFs. If OCF >0.1, the inputs were assumed to be correlated and the more complex PCFs had to be calculated. This test must be performed as a routine part of the analysis. It was found that, in some cases inputs designed to be independent were actually well correlated at certain frequencies due to structural feedback between the measurement points. When the test indicates that the inputs are correlated at some (but not all) frequencies, the problem can be broken into two parts; a frequency basis and the appropriate coherence functions (ordinary or partial) calculated for each part. If the two frequency ranges are not well separated, a practical approach would be to assume that the inputs are correlated at all

frequencies and analyze accordingly. At frequencies where this is not true, the appropriate terms will drop out and the correct solution will be obtained, at the expense of some increase in computer time.

The CF plots for this study used a linear scale for CF and a log scale for frequency, which is the format commonly found in the literature. For comparison, one plot was made with linear scales for both parameters, shown in Figure 32. Although the low frequency resolution suffers by this approach, the high frequency resolution is improved. For some applications, where the frequency range is fairly narrow, this format may be more desirable.

The effect of increasing the number of data segments used for averaging was demonstrated, using data from Run 4. The input/output OCF was plotted for 10, 50, 100, and 200 averages. It was concluded from variations in the plots that it is desirable to use 150 to 200 averages to ensure that the CF estimate is reasonably accurate, without incurring excessive computer costs. Since the duration of the data segments affects the accuracy of the results, as well as the number of segments, a trade-off between the two is necessary. A thorough investigation of this problem would be desirable, but was beyond the scope of the present study.

Another factor affecting the accuracy of the CF estimates is the windowing process applied to the test data. In this study, only rectangular windows were used (i.e., the time history was terminated abruptly at the beginning and end of each record. Improved accuracy may be gained by using more sophisticated windowing techniques, but no optimum window exists for all applications and to find the best window for coherence functions would require further study.

Phase II: Nonstationary Inputs

The ordinary coherence functions between the nonstationary inputs and the panel response appeared to vary randomly as the time period spanned by the 20 segments used for averaging was increased. Even the first case, which was calculated over a data record of only 4 seconds, resulted in OCFs that were significantly different to the OCFs for the stationary part of the run. Also, the time variation of the inputs used for the test program was fairly slow, compared with the variation experienced during a spacecraft launch for example. In Reference 5, it is shown that spacecraft vibration during liftoff will typically double in RMS level in about 4 seconds. In the test program for this study, the RMS level doubled in about 20 seconds.

This indicates that to calculate functions from flight data with reasonable confidence, very high data sampling rates would be needed so that the time duration of the data records could be minimized without incurring excessive errors. Short-time averaging techniques discussed in Reference 5, could then be applied to calculate "locally-stationary" spectral density functions, and hence, a locally-stationary version of the coherence function.

The conclusions for the study and recommendations for future studies, may be summarized as follows:

(1) For stationary data, it has been demonstrated that coherence functions can be used to identify and quantify sources of dyanmic excitation, for both correlated and noncorrelated inputs.

(2) The iterative approach formulated by Bendat for use on correlated-input systems is relatively simple to apply to a practical system.

(3) Bendat's approach is probably cheaper to run on a digital computer than the earlier matrix techniques, but side-by-side comparisons need to be made.

(4) Approximately 150 to 200 averages should be used in the computation of the auto- and cross-spectra used in the CF calculation.

(5) The use of windowing techniques on the measured data should be investigated, with the objective of reducing errors.

(6) Even for relatively slowly-varying nonstationary data, the coherence functions cannot be calculated accurately by the usual stationary data analysis techniques. More work is needed to develop practical methods for handling nonstationary data.

REFERENCES

1. Broch, J. T., "On the Applicability and Limitations of the Cross-Correlation and the Cross-Spectral Density Techniques," Bruel and Kjaer Technical Review No. 4, 1970, pp. 3-27.

2. Thaller, R. E. and Pearson, J., "Coherence Functions Used to Define Sources of Airborne Antenna Vibration," U.S. Air Force Report AFFDL-TR-78-143, December 1975.

3. Bendat, J. S., "System Identification from Multiple Input/Output Data," J. Sound & Vib., 49(3), 1976, pp. 293-308.

4. Dodds, C. J. and Robson, J. D., "Partial Coherence in Multivariate Random Processes," J. Sound & Vib., 42(2), 1975, pp. 243-249.

5. Bendat, J. S. and Piersol, A. G., Random Data: Analysis and Measurement Procedures, Wiley, 1972, pp. 136-167.

6. Potter, R., "Matrix Formulation of Multiple and Partial Coherence," J. Acoust. Soc. Am., Vol. 61, No. 3, March 1977, pp. 776-681.

7. Bendat, J. S., "Solutions for the Multiple Input/Output Problem," J. Sound & Vib., 44(3), 1976, pp. 311-325.

8. Halvorsen, W. G. and Bendat, J. S., "Noise Source Identification Using Coherent Output Power Spectra," Sound and Vibration, Vol. 8, No. 8, August, 1975.

1. Report No.	2. Government Accession No.	3. Recipient's Catalog No.
NASA CR-3142		

4. Title and Subtitle	5. Report Date
The Use of Coherence Functions To Determine Dynamic Excitation Sources on Launch Vehicle Payloads	June 1979
	6. Performing Organization Code

7. Author(s)	8. Performing Organization Report No.
Stanley Barrett and Robert M. Halvorson	MCR-78-556
	10. Work Unit No.

9. Performing Organization Name and Address	11. Contract or Grant No.
Martin Marietta Corporation P. O. Box 179 Denver, Colorado 80201	NAS1-14370
	13. Type of Report and Period Covered Contractor Report May 1977 to May 1978

12. Sponsoring Agency Name and Address	14. Sponsoring Agency Code
National Aeronautics and Space Administration Washington, D. C. 20546	

15. Supplementary Notes

Langley Technical Monitor: Brantley R. Hanks

Topical Report

16. Abstract

The problem of determining the relative contribution of simultaneous acoustic and mechanical inputs to the response of structures under combined dynamic loads was studied.

An analytical technique developed by Bendat for calculating ordinary, partial, and multiple coherence function, using an iterative nonmatrix approach was applied to data obtained from laboratory tests on a complex structural assembly. Testing was performed in an acoustically "live" room. Up to three random inputs, having similar spectral content and varying degrees of mutual coherence, and a single output were used. Stationary and nonstationary inputs were used. It was demonstrated that the technique provided an effective method of identifying sources of dynamic excitation and evaluating their relative contributions to the measured output at structural resonances, for stationary random inputs. An attempt to apply the technique to nonstationary inputs did not yield consistent results.

17. Key Words (Suggested by Author(s))	18. Distribution Statement
Coherence Functions Dynamic Loads and Environments Acoustics and Vibration	Unclassified—Unlimited Subject Category 39

19. Security Classif. (of this report)	20. Security Classif. (of this page)	21. No. of Pages	22. Price*
Unclassified	Unclassified	76	$6.00

* For sale by the National Technical Information Service, Springfield, Virginia 22161

NASA-Langley, 1979